The Journal of Experimental Biology 206, 3065-3083

doi:10.1242/jeb.00517

Aerodynamic force generation and power requirements in forward flight in a fruit fly with modeled wing motion

Mao Sun* and Jiang Hao Wu

Institute of Fluid Mechanics, Beijing University of Aeronautics & Astronautics, Beijing 100083, People's Republic of China

*Author for correspondence (e-mail: sunmao@public.fhnet.cn.net)

Accepted 27 May 2003

Summary

Aerodynamic force generation and power requirements in forward flight in a fruit fly with modeled wing motion were studied using the method of computational fluid dynamics. The Navier–Stokes equations were solved numerically. The solution provided the flow velocity and pressure fields, from which the vorticity wake structure and the unsteady aerodynamic forces and torques were obtained (the inertial torques due to the acceleration of the wing-mass were computed analytically). From the flow-structure and force information, insights were gained into the unsteady aerodynamic force generation. On the basis of the aerodynamic and inertial torques, the mechanical power was obtained, and its properties were investigated.

The unsteady force mechanisms revealed previously for hovering (i.e. delayed stall, rapid acceleration at the beginning of the strokes and fast pitching-up rotation at the end of the strokes) apply to forward flight. Even at high advance ratios, e.g. J=0.53–0.66 (J is the advance ratio), the leading edge vortex does not shed (at such advance ratios, the wing travels approximately 6.5 chord lengths during the downstroke).

At low speeds (J≈0.13), the lift (vertical force) for weight support is produced during both the down- and upstrokes (the downstroke producing approximately 80% and the upstroke producing approximately 20% of the mean lift), and the lift is contributed mainly by the wing lift; the thrust that overcomes the body drag is produced during the upstroke, and it is contributed mainly by the wing drag. At medium speeds (J≈0.27), the lift is mainly produced during the downstroke and the thrust mainly during the upstroke; both of them are contributed almost equally by the wing lift and wing drag. At high speeds (J≈0.53), the lift is mainly produced during the downstroke and is mainly contributed by the wing drag; the thrust is produced during both the down- and upstrokes, and in the downstroke, is contributed by the wing lift and in the upstroke, by the wing drag.

In forward flight, especially at medium and high flight speeds, the work done during the downstroke is significantly greater than during the upstroke. At advance ratios J≈0.13, 0.27 and 0.53, the work done during the downstroke is approximately 1.6, 2.8 and 4.2 times as much as that during the upstroke, respectively.

At J=0 (hovering), the body-mass-specific power is approximately 29 W kg^{-1}; at J=0.13 and 0.27, the power is approximately 10% less than that of hovering; at J=0.40, the power is approximately the same as that of hovering; when J is further increased, the power increases sharply. The graph of power against flying speeds is approximately J-shaped.

From the graph of power against flying speeds, it is predicted that the insect usually flies at advance ratios between zero and 0.4, and for fast flight, it would fly at an advance ratio between 0.4 and 0.53.

Key words: fruit fly, forward flight, unsteady aerodynamics, power requirement, computational fluid dynamics.

Introduction

It has been shown that quasi-steady analysis cannot predict the aerodynamic forces and power requirements of insects in hovering (Ellington, 1984b,c) or forward flight (Dudley and Ellington, 1990b; Willmott and Ellington, 1997b). Researchers have been working to shed light on the unsteady mechanisms of aerodynamic force generation and predict satisfactorily the power requirements in such cases.

Dickinson and Götz (1993) measured the aerodynamic forces on an aerofoil started impulsively at a high angle of attack in the Reynolds number (Re) range of a fruit fly wing and showed that lift was enhanced by the presence of a dynamic stall vortex, or leading-edge vortex (LEV). But lift enhancement was limited to only 2–3 chord lengths of travel because of the shedding of the LEV. For most insects, a wing section at a distance of 0.75R (where R is wing length) from the wing base travels approximately 5.3 chord lengths during an up- or downstroke in hovering flight (Ellington, 1984b); in forward flight, the section would travel an even larger distance during a downstroke.

Ellington et al. (1996) performed flow visualization studies on the hawkmoth *Manduca sexta* and a mechanical model of the hawkmoth, and discovered that on the flapping wings of the insect, the LEV did not shed during the translational phase of either up- or downstroke. Analysis of the momentum imparted to the fluid by the vortex wake showed that the LEV could explain the high lift on the insect wings. This high lift mechanism is called the delayed stall, or dynamic stall, mechanism (Ellington et al., 1996; Dickinson et al., 1999). This mechanism has been confirmed by computational fluid dynamic analysis (Liu et al., 1998). By measuring the flow field near the wings and the aerodynamic force on the wings of a mechanical model of the fruit fly *Drosophila melanogaster* (the *Re* of the fruit fly wing is 1–2 orders of magnitude smaller than that of the hawkmoth), Birch and Dickinson (2001) found that the LEV did not shed in the translational phase of either up- or downstroke and that large lift was maintained in the phase, showing that the delayed stall mechanism is valid for a wide range of *Re*.

Dickinson et al. (1999) and Sane and Dickinson (2001) conducted force measurement studies using the mechanical model of the fruit fly and showed that in the case of advanced rotation (wing rotation preceding the stroke reversal), in addition to the large lift and drag during the translatory phase of a stroke, large lift and drag peaks also occurred at the beginning and the end of the stroke (i.e. around the stroke reversal). Dickinson et al. (1999) suggested that the force peaks at the beginning of the stroke could be explained by the wake capture mechanism [an increase in the effective fluid velocity due to vortex wake shed by the previous stroke (Dickinson, 1994)], those at the end of the stroke by the rotational circulation mechanism [the lift due to wing rotation is related to the rotational circulation by the Kutta–Jukowski equation and the rotational circulation is determined by the Kutta condition as being proportional to the product of the rotation rate and the distance between rotation-axis and 0.75 chord position (Fung, 1969)]. They provided evidence for the wake capture by flow visualizations made at the start of a stroke and by force measurements after halting the wing at the start of a stroke. Dickinson et al. (1999) and later, Sane and Dickinson (2002), assumed that the total force (lift and drag) due to the wing rotation (rotational force) could be related to the rotational circulation by the Kutta–Jukowski equation, and using measured rotational force, they determined the rotational circulation as a function of the rotation rate and the rotation-axis position. The experimentally determined rotational circulation agreed reasonably well with that predicted by Fung's theory (Fung, 1969), providing evidence that force peaks near the end of the stroke were due to rotational circulation.

Using the method of computational fluid dynamics (CFD), Sun and Tang (2002a) simulated the unsteady flow around a model fruit fly wing conducting flapping motions similar to that in the experiment of Dickinson et al. (1999). Different, but complementary, explanations for the force peaks were provided. By varying the acceleration at the beginning of a stroke, it was found that the force peaks there were closely related to the acceleration. From the computed flow field, it was observed that during the fast acceleration of the wing, strong vorticity was continuously generated on the lower wing surface and shed at the trailing edge, while strong vorticity of opposite sign was continuously generated at the upper wing surface. From vorticity dynamics theory (Wu, 1981), this would give rise to a large time rate of change of vorticity moment and thus large forces. If the velocity due to the previous strokes was directed towards the wing at the start of the stroke, wake capture mechanism would also contribute to the force peaks. But the computed results showed that the velocity was directed downward. Therefore, the authors suggested that the large force peaks at the beginning of the stroke could be explained by the rapid generation of strong vorticity due to the fast translational acceleration of the wing. However, it should be noted that the computed flow field in front of the wing at the start of a stroke is different from that visualized experimentally (Dickinson et al., 1999; the later shows the existence of wake capture effect and the former does not), and that although the computed forces are generally in agreement with the measured, there are noticeable discrepancies around the stroke reversal [see the comparisons in Sun and Tang (2002b) and in the 'validation' section of the present paper]. Thus there exists the possibility that the CFD simulations could not capture accurately all features of the flow. During the fast pitching-up rotation near the end of the stroke, it was also observed that new vorticity of large strength was produced. The authors suggested that the large force peaks near the end of the stroke could be explained by the rapid generation of strong vorticity due to the fast pitching-up rotation of the wing. Note that the rotational circulation approach (Dickinson et al., 1999; Sane and Dickinson, 2002) is a special case of the vorticity dynamics theory; under conditions that the flow is quasi-steady and inviscid, the equations in the rotational circulation approach can be derived from the vorticity dynamics theory. Therefore, the above explanation for the wing rotation effects is complementary to that based on the rotational circulation approach.

As a result of the above works and numerous others (e.g. Vogel, 1966; Weis-Fogh, 1973; Ellington, 1984a,b, 1995; Ennos, 1989; Dudley and Ellington, 1990a,b; Willmott et al., 1997; Wang, 2000), we are now better able to understand how insects produce large lift.

With the current understanding of the unsteady force production mechanisms, researchers have attempted to estimate the mechanical power of insect flight based on unsteady aerodynamic forces. Sane and Dickinson (2001), using the measured unsteady drag of a model fruit fly wing, showed that the mechanical power for a fruit fly was approximately twice as much as the previous estimate based on quasi-steady theory (Lehmann and Dickinson, 1997). Recently, Sun and Tang (2002b), through unsteady flow simulation by the CFD method, studied the lift and power requirements of hovering flight in the fruit fly. Under conditions where the mean lift balanced the insect weight, they

computed the required mechanical power. With the computed mechanical power and available metabolic data, a value of 0.17 for the muscle efficiency was obtained, and was approximately twice as much as that estimated using the quasi-steady theory (0.09; Lehmann and Dickinson, 1997).

Though the above works on unsteady mechanisms of force production and power requirements were primarily concerned with hovering flight, it is believed that the unsteady mechanisms of force production are also applicable to the case of forward flight. In fact, flow visualization experiments on the tethered hawkmoth (Ellington et al., 1996; Willmott et al., 1997) have already shown that the delayed stall mechanism operates at advance ratios ranging from 0 to 0.9. However, the flow visualization results for the tethered insect were not so clear-cut because of the difficulty in obtaining good flow visualization near the wings. It is of interest to investigate the flow around the flapping wings during forward flight in more detail. For the power requirements in forward flight, Ellington et al. (1990), measured the oxygen consumption of bumblebees and showed that the metabolic power changed little from hovering to intermediate flight speeds. Assuming that muscle efficiency was constant over different flight speeds, it was concluded that the mechanical power would vary with the flight speed according to a J-shaped curve (Ellington et al., 1990; Ellington, 1991). It is of great interest to calculate the mechanical power directly and to see how it varies with the flight speed.

We here investigate these problems using a virtual fruit fly. Systematic kinematic data on free-flying fruit flies are not available at present. Assumptions on the wing motion and its variation with flight speed are made on the basis of existing data from tethered and free-flying fruit flies and some data from other insects. The method of computational fluid dynamics is used in the study. In the method, the pressure and velocity fields around the flapping wing are obtained by solving the Navier–Stokes equations numerically; the lift and thrust and the torques due to the aerodynamic forces are calculated based on the flow pressure and velocities. The inertial torques due to the acceleration and rotation of the wing-mass are calculated analytically. From the aerodynamic and inertial torques, the mechanical power required for the flight is calculated.

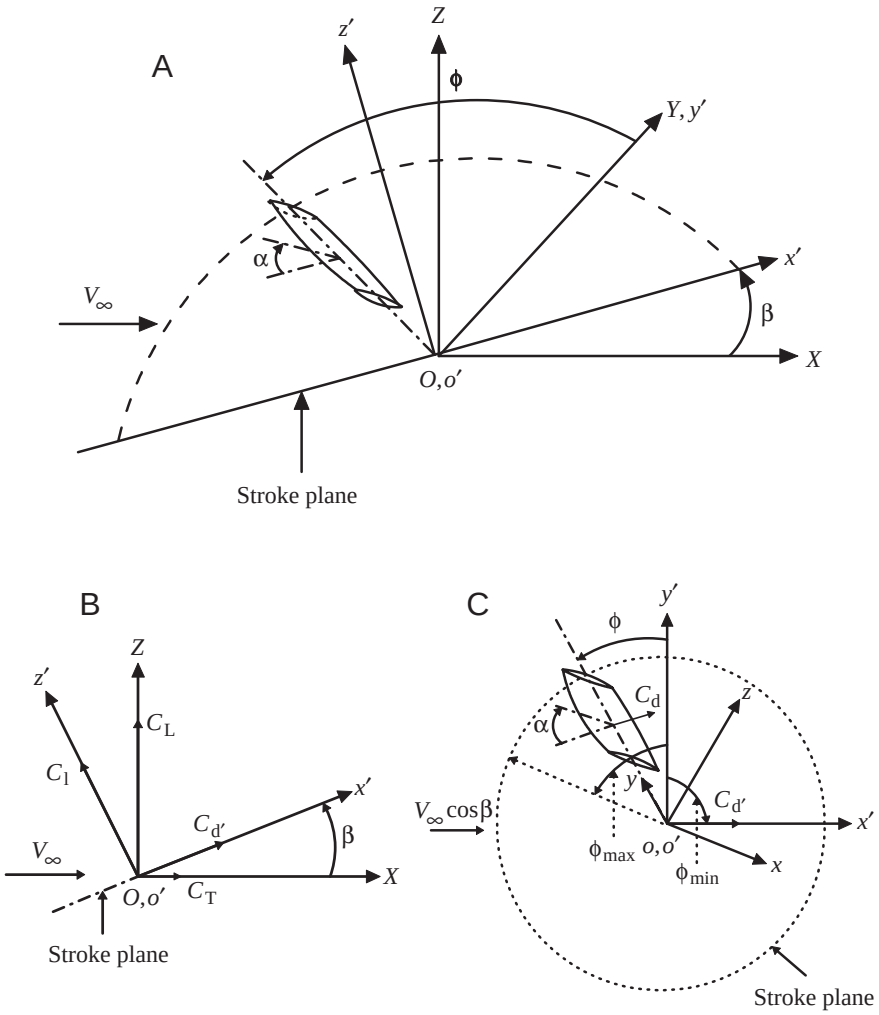

Fig. 1. Sketches of the reference frames and wing motion. *OXYZ* is an inertial frame, with the *XY* plane in the horizontal plane. $o'x'y'z'$ is another inertial frame, with the $x'y'$ plane in stroke plane. *oxyz* is a frame fixed on the wing, with the *x* axis along the wing chord, and the *y* axis along the wing span. ϕ, positional angle of the wing; ϕ_{min} and ϕ_{max}, minimum and maximum positional angle, respectively; α, angle of attack of the wing; β, stroke plane angle; V_∞, free-stream velocity; and *R*, wing length. C_L and C_T, coefficients of lift and thrust, respectively; C_l and C_d, coefficients of wing lift and wing drag, respectively; $C_{d'}$, x' component of C_d.

Materials and methods

The wing and the coordinate systems

The wing considered in the present study is the same as that used in the study of fruit fly lift and power requirements in hovering flight (Sun and Tang, 2002b). The planform of the wing is similar to that of a fruit fly wing and the wing section is an ellipse whose thickness is 12% of the aerofoil chord length, and the radius of the leading and trailing edges is 0.2% of the aerofoil chord length. The radius of the second moment of wing area, r_2, is 0.58*R*, where *R* is the wing length (the mean flapping velocity at span location r_2 is used as reference velocity in the present study).

Three coordinate systems are used. Two are inertial coordinate systems, *OXYZ* and $o'x'y'z'$. For *OXYZ*, the origin *O* is at the wing base (see Fig. 1A); *X* and *Y* form the horizontal plane (*X* is in the direction of the free stream velocity), and the *Z*-direction is

vertical. The coordinate system $o'x'y'z'$ has the same origin as the coordinate system *OXYZ*, its y' axis coincides with the Y axis, and its $o'x'y'$ plane coincides with the stroke plane (see Fig. 1A,B). The third is the body-fixed coordinate system *oxyz*. It has the same origin as the two inertial coordinate systems, but it rotates with the wing. The x axis is parallel to the wing chord and the y axis is on the pitching-rotation axis of the wing (see Fig. 1C). The free-stream velocity, which has the same magnitude as the flight velocity, is denoted by V_∞, and the stroke plane angle denoted by β (see Fig. 1A).

The flow computation method

The flow equations and computational method used in the present study are the same as those in Sun and Tang (2002a,b). Only an outline of the method is given here. The Navier–Stokes equations are solved using the algorithm developed by Rogers and Kwak (1990) and Rogers et al. (1991), which is based on the method of artificial compressiblity. The algorithm uses a third-order flux-difference splitting technique for the convective terms and the second-order central difference for the viscous terms. The time derivatives in the momentum equation are differenced using a second-order, three-point, backward-difference formula. The algorithm is implicit and has second-order spatial and time accuracy.

Evaluation of the aerodynamic forces, aerodynamic and inertial torques and mechanical power

Once the Navier–Stokes equations are numerically solved, the fluid velocity components and pressure at discretized grid points for each time step are available. The aerodynamic forces and torques acting on the wing are calculated from the pressure and the viscous stress on the wing surface. The inertial torques due to the acceleration of the wing-mass are calculated analytically.

The wing lift l is the component of the total aerodynamic force perpendicular to the translational velocity of the wing (defined below), i.e. perpendicular to the stroke plane, and is positive when it is in the positive z' direction (see Fig. 1B). The wing drag d is the component of the total aerodynamic force parallel to the translational velocity and is positive when directed opposite to the direction of the translational velocity of the downstroke (see Fig. 1C). (The wing drag is the force that the insect must overcome for the translational motion of its wing and is relevant to the power requirement of flight.) The x' component of d is denoted as d', and $d'=d\cos\phi$, where ϕ is the positional angle of the wing (see Fig. 1C). Resolving the wing lift l and the force d' into the Z and X axes, we obtain the lift L (vertical force) and the thrust T, respectively (see Fig. 1B,C): $L=l\cos\beta+d'\sin\beta$ and $T=l\sin\beta-d'\cos\beta$. The coefficients of the above force components are defined as follows:

$$C_L = \frac{L}{0.5\rho U^2 S}, \tag{1}$$

$$C_T = \frac{T}{0.5\rho U^2 S}, \tag{2}$$

$$C_l = \frac{l}{0.5\rho U^2 S}, \tag{3}$$

$$C_{d'} = \frac{d'}{0.5\rho U^2 S}, \tag{4}$$

$$C_d = \frac{d}{0.5\rho U^2 S}, \tag{5}$$

where ρ is the fluid density, U is the reference velocity (defined below), and S is the wing area. The formulae for the aerodynamic and inertial torques and the mechanical power were given in Sun and Tang (2002b) and will not be repeated here.

Kinematics of the flapping wings

As noted by Dickinson et al. (1999), a down- or upstroke of an insect is typically divided into three portions: pitching-down rotation and translational acceleration at the beginning of the stroke, translation at constant speed and constant angle of attack during the middle of the stroke, and pitching-up rotation and translational deceleration at the end of the stroke. This simplified flapping pattern is employed here. It is assumed that the geometric angle of attack and the duration of the upstroke are the same as that of the downstroke, respectively [Vogel's observation (Vogel, 1967) shows that this is approximately true for tethered *Drosophila virilis* in forward flight]. The flapping motion is modeled as follows. The azimuthal rotation of the wing about the z' axis, which is normal to the stroke plane (see Fig. 1A), is called translation, and the pitching rotation of the wing near the end of a stroke and at the beginning of the following stroke is called rotation or flip. The translational velocity is denoted by u_t, which takes a constant value of U_m except at the beginning and near the end of a stroke. During the acceleration at the beginning of a stroke, u_t is given by:

$$u_t^+ = U_m^+ \sin[\pi(\tau-\tau_0)/\Delta\tau_t]; \qquad \tau_0 \leqslant \tau \leqslant [\tau_0 + (\Delta\tau_t/2)], \tag{6}$$

where the non-dimensional translational speed of the wing $u_t^+=u_t^+/u$ (U is the reference velocity, defined below), u_m^+ (the maximum of u_t^+)$=U_m/U$, $\tau=tU/c$ (t is dimensional time, c is the mean chord length the wing and τ is the non-dimensional time), τ_0 is the non-dimensional time at which the stroke starts and $\tau_0+(\Delta\tau_t/2)$ the time at which the acceleration at the beginning of the stroke finishes. $\Delta\tau_t$ is the duration of deceleration/acceleration around stroke reversal. Near the end of the stroke, the wing decelerates from $u_t^+=U_m$ to $u_t^+=0$, according to:

$$u_t^+ = U_m^+ \sin\left\{\frac{\pi}{\Delta\tau_t}[\tau - \tau_1 + (\Delta\tau_t/2)]\right\}; \qquad \tau_1 \leq \tau \leq [\tau_1 + (\Delta\tau_t/2)], \tag{7}$$

where τ_1 is the non-dimensional time at which the deceleration starts. The azimuth-rotational speed of the wing is related to u_t. Denoting the azimuthal-rotational speed as $\dot{\phi}$, we have $\dot{\phi}(\tau)=u_t/r_2$. The geometric angle of attack of the wing is denoted

by α. It also takes a constant value except at the beginning or near the end of a stroke. The constant value is denoted by α_m, midstroke angle of attack. Around the stroke reversal, α changes with time and the angular velocity, $\dot{\alpha}$, is given by:

$$\dot{\alpha}^+ = 0.5\dot{\alpha}_0^+ \{1 - \cos[2\pi(\tau - \tau_r)/\Delta\tau_r]\} ; \quad \tau_r \leqslant \tau \leqslant (\tau_r + \Delta\tau_r) , \quad (8)$$

where the non-dimensional form, $\dot{\alpha}^+=\dot{\alpha}/U$, $\dot{\alpha}_0^+$ is a constant, and τ_r is the non-dimensional time at which the rotation starts, $\Delta\tau_r$ the non-dimensional time interval over which the rotation lasts. In the time interval of $\Delta\tau_r$, the wing rotates from $\alpha=\alpha_m$ to $\alpha=180°-\alpha_m$. Therefore, when α_m and $\Delta\tau_r$ are specified, $\dot{\alpha}_0^+$ can be determined (around the next stroke reversal, the wing would rotate from $\alpha=180°-\alpha_m$ to $\alpha=\alpha_m$, so the sign of the right-hand side of Equation 8 should be reversed). It is assumed that the axis of the pitching rotation is located at 0.2*c* from the leading edge of the wing. $\Delta\tau_r$ is the wing rotation duration (or flip duration).

In the flapping motion described above, the reference velocity *U*, the velocity at midstroke U_m, the geometric angle of attack at midstroke α_m, the deceleration/acceleration duration $\Delta\tau_t$, the wing rotation duration $\Delta\tau_r$, the flip timing τ_r, the period of flapping cycle τ_c and the stroke plane angle β must be specified.

Ennos (1989) made observations of free forward flight of two fruit flies *Drosophila melanogaster*, one at advance ratio 0.16 and the other at advance ratio 0.33. Ellington (1984a) made observations of free hovering flight of craneflies, hoverflies and droneflies (and many other insects). Their data show that the deceleration/acceleration duration $\Delta\tau_t$ and the duration of wing rotation $\Delta\tau_r$ are approximately $0.2\tau_c$, and that wing rotation is symmetrical. It is assumed here that $\Delta\tau_t=0.18\tau_c$ and $\Delta\tau_r=0.24\tau_c$ (these values were used in previous work on fruit fly lift and power requirements in hovering flight; Sun and Tang, 2002b) and that the wing rotation is symmetrical (as a result, τ_r may be determined).

To determine the reference velocity *U* and some other parameters, data in the previous study on free hovering in *Drosophila virilis* (Sun and Tang, 2002b) are used again here. These data were taken from Weis-Fogh (1972, 1973) and they are as follows: insect weight is 1.96×10^{-5} N, wing length *R* is 0.3 cm, area of both wings S_t is 0.058 cm^2, stroke amplitude Φ is 150°, and stroke frequency *n* is 240 s^{-1}. The reference velocity is determined as $U(=2\Phi nr_2)=218.7$ cm s^{-1} (for all cases considered in the present study, the reference velocity, reference length and reference time are fixed as $U=218.7$ cm s^{-1}, $c=0.108$ cm and $c/U=0.495\times10^{-3}$ s).

To determine U_m^+ and τ_c (U/nc), data on how the stroke amplitude and stroke frequency vary with flight speed are needed. They are not available for fruit flies in free flight. Studies on the free flight of bumblebees (Dudley and Ellington, 1990a) and the hawkmoth (Willmott and Ellington, 1997a) showed that for both insects, the stroke frequency was constant. For bumblebees, the stroke amplitude did not vary significantly, but for the hawkmoth, the stroke amplitude varied with flight speed. Studies on tethered *Drosophila virilis* (Vogel, 1967) showed that the stroke frequency was constant and the stroke amplitude varied with flight speed. But in tethered *D. melanogaster*, Lehmann and Dickinson (1997) showed that both frequency and stroke amplitude changed with flight force. In the present study, we examine three different cases. (1) It is assumed that the stroke amplitude and stroke frequency do not vary with flight speed ($\Phi=150°$ and $n=240$ s^{-1}). (2) The stroke amplitude is allowed to vary with flight speed and is determined by force balance condition (frequency kept constant, $n=240$ s^{-1}). (3) The frequency is allowed to vary with flight speed and is determined by force balance condition (stroke amplitude kept constant, $\Phi=150°$).

α_m and β remain to be determined. They are determined by the force balance condition, i.e. mean lift is equal to insect weight and mean thrust is equal to the insect body drag. The weight of the insect is given above. The body drag in *Drosophila virilis*, as a function of body angle, was measured by Vogel (1966) for five flight speeds, ranging from 0.5 to 2.5 m s^{-1}. In the present study, we examine forward flight at these flight speeds and used Vogel's body-drag data [fig. 5 in Vogel, 1966). It is assumed the angle between the stroke plane and the longitudinal body axis is constant [data in *Drosophila virilis* in tethered flight (Vogel, 1967) and in other flies (Ellington, 1984a) show that this is approximately true]. On the basis of Vogel's data in *Drosophila virilis* in tethered flight, the body angle χ is related to stroke plane angle β as follows (Vogel, 1966):

$$\chi = 68° - \beta . \quad (9)$$

The Reynolds number *Re* and the mean lift coefficient required for supporting the insect weight $\overline{C_{L,w}}$ are calculated as follows: $Re=cU/\nu=147$ ($\nu=147$ cm^2 s^{-1}); $\overline{C_{L,w}}=1.96\times10^{-5}$ N/$0.5\rho U^2S_t=1.15$ ($\rho=1.23\times10^{-3}$ g cm^{-3}). The advance ratio *J* is defined as $J=V_\infty/(UR/r_2)$, and in the present study, it ranged from 0.13 to 0.66 (when presenting the results in later sections, some results for hovering flight, $J=0$, are also included).

Results and Discussion

Validation

The code used here is the same as that in the study of fruit fly lift generation and power requirements in hovering flight (Sun and Tang, 2002a,b). It is based on the flow computation method outlined above, and was developed by Lan and Sun (2001a). It was verified by the analytical solutions of simple flows [boundary layer flow on a flat plate (Lan and Sun, 2001a); flow at the beginning of a suddenly started aerofoil (Lan and Sun, 2001b)] and tested by measured steady-state pressure distributions on a wing (Lan and Sun, 2001a).

In earlier studies (Sun and Tang, 2002b), the code was tested by measured unsteady aerodynamic forces on a model fruit fly wing in flapping motion (Dickinson et al., 1999; the wing geometry was obtained from Prof. M. H. Dickinson). Three cases of wing rotation timing were considered (the stroke amplitude was 160° and the midstroke geometric angle of attack was 40°), but only the lift forces were compared. In a

recent paper by Sane and Dickinson (2001), both lift and drag on the same model wing are given for a wide range of wing kinematic parameters. Here, we make further comparisons between calculations and experiments, using the data of Sane and Dickinson (2001). The computed and measured lift and drag coefficients are shown in Fig. 2 [for results in Fig. 2A,B, the stroke amplitude is 60° and the midstroke geometric angle of attack is 50°; for results in Fig. 2C,D, these parameters have values of 180° and 50°, respectively; experimental data are taken from fig. 3C,D of Sane and Dickinson (2001)].

The calculated drag coefficient agrees well with the measured (see Fig. 2A,C). For the lift coefficient (see Fig. 2B,D), in the translational phase of the downstroke, the computed value agrees well with the measured; around the stroke reversal, the computed peak values are smaller than the measured; in the translational phase of the upstroke, the computed value is a little less than the measured, but they are in qualitative agreement (note that the value of the measured lift coefficient in the upstroke is higher than that in the downstroke). The above is also true in the lift coefficient comparisons in Sun and Tang (2002b) [see fig. 4 of Sun and Tang (2002b); there the downstroke was plotted as the second half of the flapping cycle].

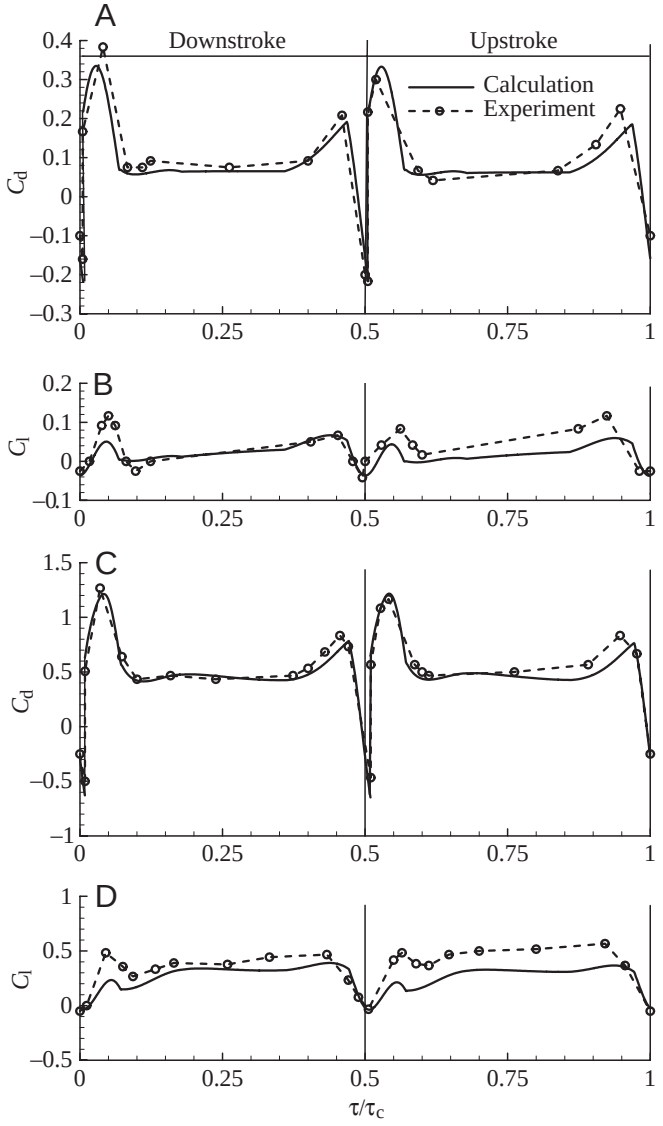

Fig. 2. Comparison of the calculated and measured lift (C_L) and drag (C_d) coefficients. The experimental data are reproduced from fig. 3C,D of Sane and Dickinson (2001). (A,B) The midstroke angle of attack α_m is 50° and stroke amplitude Φ_h is 60°. (C,D) The midstroke angle of attack α_m is 50° and stroke amplitude Φ_h is 180°. τ, non-dimensional time; τ_c, non-dimensional period of one flapping cycle.

The above comparisons show that although the CFD simulations might not capture accurately all the flow features around the stroke reversal, the agreement of the aerodynamic force coefficients between the computational and experimental simulations is reasonably good. We think that the present CFD method can calculate the unsteady aerodynamic forces and torques of the model insect wing with reasonable accuracy.

In the above calculations, the computational grid has dimensions 93×109×71 in the normal direction, around the wing section and in the spanwise direction, respectively. The normal grid spacing at the wall was 0.002. The outer boundary was set at 10 chord lengths from the wing. The time step was 0.02. Detailed studies of the numerical variables such as grid size, domain size, time step, etc., were conducted in our previous work on the unsteady lift mechanism of a flapping fruit fly wing (Sun and Tang, 2002a,b), where it was shown that the above values for the numerical variables were appropriate for the flow calculation. Therefore, in the following calculation, the same set of numerical variables is used.

Force balance in forward flight

Since we wished to study the aerodynamic force and power requirements for balanced flight, we first investigated the force balance. In the study of hovering flight by Sun and Tang (2002b), there was no body drag. The stroke plane was assumed to be horizontal (β=0) and the mean thrust was zero, therefore the horizontal force was balanced. The midstroke angle of attack α_m was adjusted such that the weight of the insect was balanced by the mean lift.

In forward flight, the body drag is not zero and the stroke plane is tilted forward to produce thrust. At a given flight speed or advance ratio, for different values of α_m and β, the mean lift and mean thrust are different (the stroke amplitude Φ and stroke frequency n were assumed to be constant). α_m and β at a given flight speed are determined using the force balance condition (mean lift equals the weight and mean thrust equals the body drag).

The calculation procedure is as follows. A flight speed is specified. A set of values for α_m and β is guessed; the flow equations are solved and the corresponding mean lift and thrust coefficients $\overline{C_L}$ and $\overline{C_T}$ are calculated. The body drag for the given flight speed and body angle (body angle is related to β by Equation 9) is obtained from Vogel (1966). The $\overline{C_L}$ was compared with $\overline{C_{L,W}}$ and the mean thrust (=$0.5\rho\overline{U^2}S_t\overline{C_T}$) is compared with the body drag. If $\overline{C_L}$ is not equal to $\overline{C_{L,W}}$ or the

Table 1. *Mean lift ($\bar{C}_L$) and thrust ($\bar{C}_T$) coefficients, midstroke angle of attack α_m, stroke plane angle β, body angle χ and coefficient of work per cycle C_w as functions of advance ratio* J

J	$\bar{C}_L$	$\bar{C}_T$	α_m (deg.)	β (deg.)	χ (deg.)	C_w	$C^+_{W,t}$	$C^-_{W,t}$	$C^+_{W,r}$	$C^-_{W,r}$
0	1.16	0.03	36	0	68	12.91	12.51	–0.75	0.40	–1.82
0.13	1.16	0.04	32	16.5	51.5	11.50	10.90	–0.46	0.60	–1.40
0.27	1.16	0.09	34	29	39	11.47	10.93	–0.43	0.53	–1.32
0.40	1.15	0.15	43.5	45.5	22.5	13.58	13.37	–0.70	0.21	–1.69
0.53	1.15	0.20	56	60	8	18.21	18.16	–0.93	0.05	–1.80

α_m, β vary with flight speed; stroke amplitude Φ=150°; stroke frequency n=240 s^{-1} and non-dimensional period τ_c=8.42.
$C^+_{W,t}$ and $C^-_{W,t}$, coefficients of positive and negative work for translation, respectively; $C^+_{W,r}$ and $C^-_{W,r}$, coefficients of positive and negative work for rotation, respectively.

mean thrust is not equal to the body drag, then α_m and β are adjusted [the gradients of $\overline{C_L}$ (and $\overline{C_T}$) with respect to α_m and β are used as markers for adjusting α_m and β]; and the calculations are repeated until the magnitudes of difference between $\overline{C_L}$ and $\overline{C_{L,W}}$ and between $\overline{C_T}$ and body drag (divided by $0.5\rho U^2 S_t$) are less than 0.01.

The calculated results for four forward flight speeds are shown in Table 1 (the results for hovering flight are also included). It is seen that $\overline{C_L}$ is close to 1.15, as it should be. $\overline{C_T}$ increases almost linearly with flight speed, as does the body drag. (For a fixed body angle, the drag would increase more rapidly than linearly with flight speed; but here the body angle decreased with flight speed.) α_m is close to that that of hovering flight at small and medium speeds (J=0.13, 0.27; V_∞=0.5, 1.0 m s^{-1}) but increases to large values at higher speeds. β increases almost linearly with flight speed. From the ratio between $\overline{C_T}$ and $\overline{C_L}$, the orientation of the total force vector can be calculated. At hovering, β=0, and the total force vector is vertical; at medium speed (J=0.27; V_∞=1.0 m s^{-1}), β=29°, and the total force vector tilts forward by 4.4°; at high speed (J=0.53; V_∞=2.0 m s^{-1}), β=60°, and the total force vector tilts forward by 10°.

It should be noted that calculated results are not given for J=0.66 or V_∞=2.5 m s^{-1} (at which flight speed body drag is available). At this flight speed, no matter how α_m and β are adjusted, enough lift cannot be obtained. (As will be seen below, at this flight speed, if the stroke amplitude is increased, enough lift can be obtained, but the power required would be very large.)

The generation of the lift and thrust

Here, we investigate how the lift and the thrust on the insect are generated.

The lift (vertical force) and thrust

Fig. 3B,C gives the lift (C_L) and thrust (C_T) coefficients *versus* non-dimensional time in a flapping cycle for five advance ratios, J=0, 0.13, 0.27, 0.40 and 0.53 (V_∞=0, 0.5, 1.0, 1.5 and 2.0 m s^{-1}). (The mean values of the force coefficients have been given in Table 1.)

As seen in Fig. 3B,C, at low flight speed (J=0.13), C_L in the upstroke is smaller than that in the downstroke; both down- and upstroke contribute to the mean lift, but approximately 75% of it is from the downstroke. Negative thrust is produced in the downstroke and positive thrust in the upstroke, but the amount of the positive thrust in the upstroke is larger than that of negative thrust in the downstroke, resulting in a positive mean thrust. Therefore, the mean thrust is contributed by the upstroke (the downstroke has negative contribution).

At medium flight speed (J=0.27), C_L is large in the downstroke but very small in the upstroke, so the mean lift is mainly contributed by the downstroke. Similar to the case of low speed, the mean thrust is contributed by the upstroke (the downstroke has negative contribution).

At high flight speed (J=0.53), C_L in the downstroke is even larger, and C_L in the upstroke is negative but is of small magnitude. Therefore, the mean lift is contributed by the downstroke (the upstroke has negative contribution). Positive thrust is produced in the downstroke (because in this case, the stroke plane angle is large, β=60°), and relatively large positive thrust is produced in the upstroke; approximately 74% of the mean thrust is from the upstroke.

The lift and thrust coefficients (C_L and C_T, respectively) shown above are the results of the wing lift and wing drag coefficients (C_l and C_d, respectively). In fact, only the x' component of C_d ($C_{d'}$; see Fig. 1B,C) contributes to C_L and C_T (C_d is relevant to the aerodynamic power of the wing). The corresponding C_l, C_d and $C_{d'}$ values are shown in Fig. 3D–F.

At low speed (J=0.13), as shown above, 75% and 25% of the mean lift are contributed by the downstroke and the upstroke, respectively. In most of the downstroke, the magnitudes of C_l and C_d are approximately the same. Since β is not very large (β=16.5°), the major part of C_L is from C_l, and approximately 20% of C_L is from $C_{d'}$. In the upstroke, $C_{d'}$ has negative contribution to C_L. Also as shown above, the mean thrust is contributed by the upstroke; in the upstroke, it is $C_{d'}$ that gives the major portion of the thrust, and C_l contributes approximately 20% of C_T. Therefore, it can be stated that the mean lift is contributed by the wing lift of both the down- and upstrokes (the contribution of downstroke is approximately three times as large as that of upstroke), and that the mean thrust is contributed mainly by the x' component of the wing drag of the upstroke.

At medium flight speed (J=0.27), as shown above, the mean lift is contributed mainly by the downstroke and the mean thrust is contributed by the upstroke. In the downstroke, C_l and $C_{d'}$ have same sign and are approximately of the same magnitude (around 1.8), and in the upstroke, C_l is mostly positive and $C_{d'}$ is negative, and they are also approximately of the same magnitude. Noting that β is about 30°, it can be stated that the mean lift is contributed almost equally by the wing lift and the x' component of the wing drag of the downstroke, and that the mean thrust is contributed almost equally by the wing lift and the x' component of the wing drag of the upstroke.

At high flight speed (J=0.53; α_m=56°, β=60°), based on similar analysis, it can be stated that the mean lift is contributed mainly by the the x' component of the wing drag of the downstroke (note the similarity between $C_{d'}$ in Fig. 3F and C_L in Fig. 3B during the downstroke), and that a relatively large part of the mean thrust is contributed by the x' component of the wing drag of the upstroke and a relatively small part of the mean thrust is contributed by the wing lift of the downstroke.

The mechanism of the generation of the wing lift and drag

The mechanisms of unsteady force production by the model fruit fly wing in the case of hovering flight were studied by Dickinson et al. (1999) and Sun and Tang (2002a). It was shown that (for symmetrical rotation) the peak in C_d and the dip in C_l at the beginning of a down- or upstroke (see C_l and C_d for J=0 in Fig. 3D,E) were due to the combined effects of acceleration and rotation of the wing; the large C_l and C_d (around 1.2) during the translational phase of the down- or upstroke were due to the delayed stall mechanism, and the peaks in C_l and C_d near the end of the down- or upstroke were due to the pitching-up rotation of the wing.

In the case of forward flight, as shown in Fig. 3D,E, the C_l and C_d peaks near the end of the strokes and the C_d peak and C_l dip at the beginning of the strokes still exist and are similar to those in the case of hovering flight. This is because at the

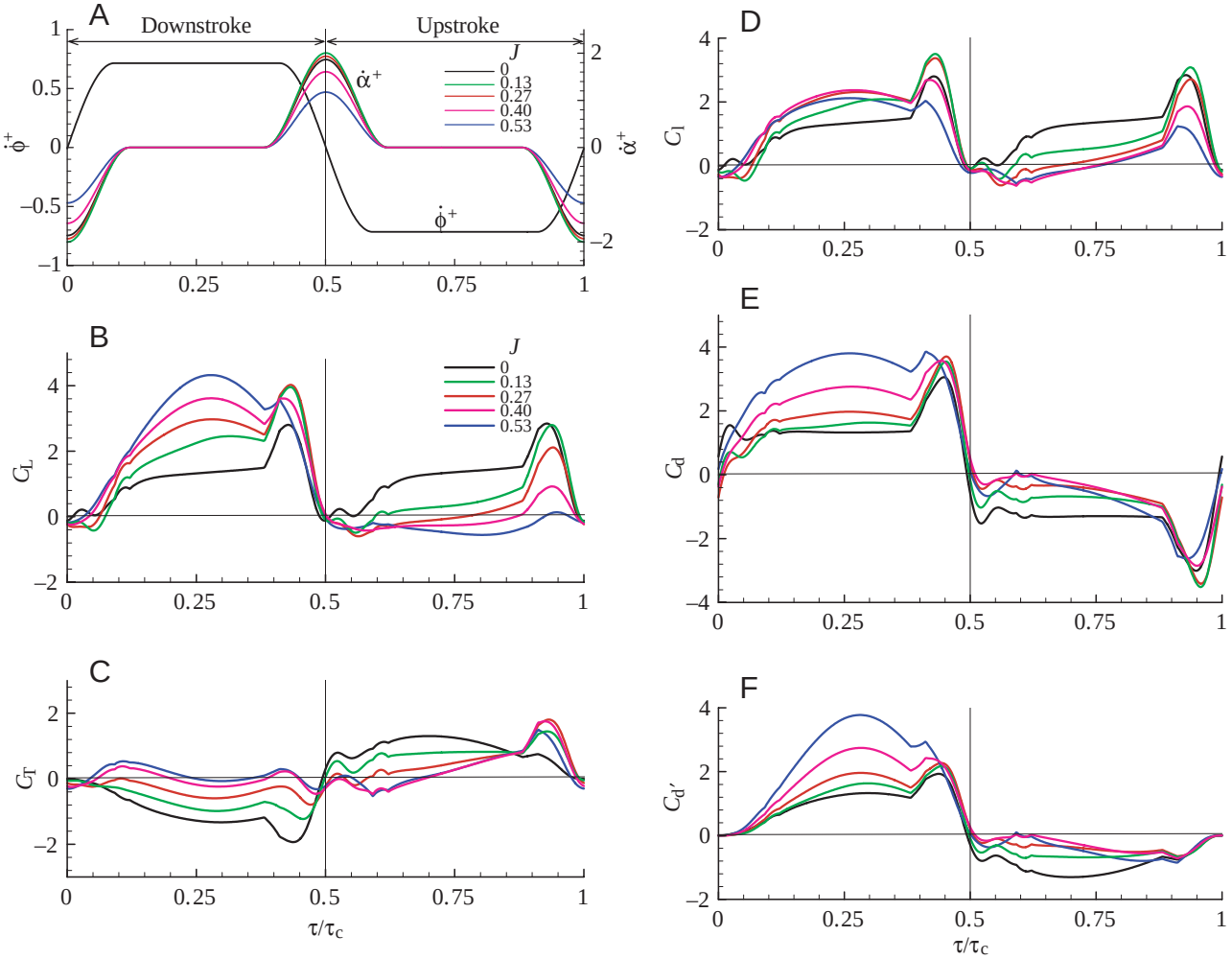

Fig. 3. Non-dimensional angular velocity of pitching rotation $\dot{\alpha}^+$ and azimuthal rotation $\dot{\phi}^+$ (A), lift coefficient C_L (B), thrust coefficient C_T (C), wing lift coefficient C_l (D), wing drag coefficient C_d (E) and x' component of wing drag coefficient $C_{d'}$ (F) *versus* time during one cycle for five advance ratios J. τ_c, non-dimensional period of one flapping cycle; τ, non-dimensional time (midstroke angle of attack α_m and stroke plane angle β vary with flight speed; stroke amplitude Φ_h=150°).

beginning or the end of a stroke, the positional angle of the wing is either near ϕ_{min} or ϕ_{max} (see Fig. 1C) where the component of the free-stream velocity that is normal to the wing span is small, and as a result the free-stream velocity has very limited effect on the force production of the wing there. The difference in size of the peaks for various advance ratios were mainly caused by the difference in rotation rate of the wing. Therefore, the force production mechanisms at the beginning and near end of the strokes in forward flight are the same as that in hovering flight.

We now consider C_l and C_d in the translatory phase of the down- or upstroke (the middle 64% of the down- or upstroke). In order to assist the analysis of the force coefficients, the contours of the non-dimensional spanwise component of vorticity at mid-span location are given in Figs 4–6 for J=0, 0.27 and 0.53, respectively, and the corresponding sectional streamline plots (seen in the body-fixed frame *oxyz*) are given in Figs 7–9.

For the case of medium flight speed (J=0.27; β=29°; α_m=34°), during the translatory phase of the downstroke (τ=0.09~0.41τ_c), similar to the case of hovering, both C_l and C_d maintain large and almost constant values (see Fig. 3D,E). From Fig. 5B–D (and Fig. 8A–C), it is seen that during this period, the LEV does not shed. Therefore, maintaining the large C_l and C_d during this period is due to the delayed stall mechanism. C_l is approximately 2.1 and C_d approximately 1.8. Both are larger than in hovering flight (approximately 1.4 and 1.2, respectively). This is because during the downstroke of forward flight, due to the free-stream velocity, the wing sees a relative velocity that has a larger magnitude and a slightly smaller effective angle of attack (the z' component of V_∞ acting to decrease the effective angle of attack). During the translatory phase of the upstroke (τ=0.59~0.91τ_c), both C_l and C_d are much smaller than that of hovering

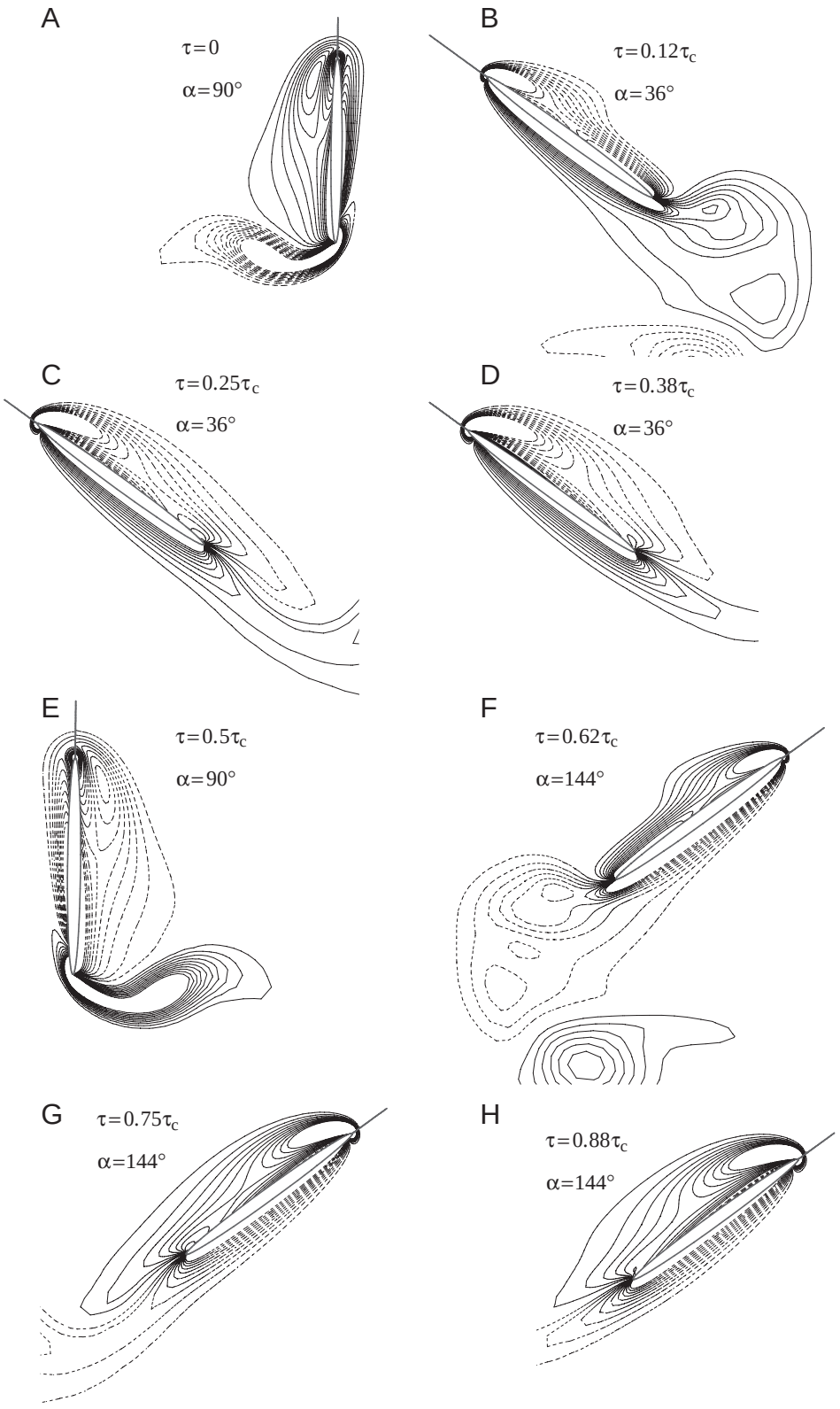

Fig. 4. (A–H) Vorticity plots at half-wing length at various times during one cycle (advance ratio J=0). τ, non-dimensional time; τ_c, non-dimensional period of one cycle; α, angle of attack of wing. Solid and broken lines indicate positive and negative vorticity, respectively. The magnitude of the non-dimensional vorticity at the outer contour is 1 and the contour interval is 1. (A–D), downstroke; (E–H), upstroke.

flight. This is because during the upstroke, the wing sees a relative velocity that has a smaller magnitude and a smaller effective angle of attack (in the upstroke, since the magnitude of the relative velocity is small, the same z' component of V_∞ causes a greater decrease in effective angle of attack than in the downstroke). Comparing the streamline plots for J=0.27 in Fig. 8D–F and that for J=0 in Fig. 7D–F, it is seen that the streamlines in front of the wing for J=0.27 have a much smaller angle of attack than that for J=0. From Fig. 5D–F, it is interesting to see that during the upstroke of forward flight, due to the smaller effective angle of attack, the vorticity on the upper surface of the wing is only a little different from that on the lower surface.

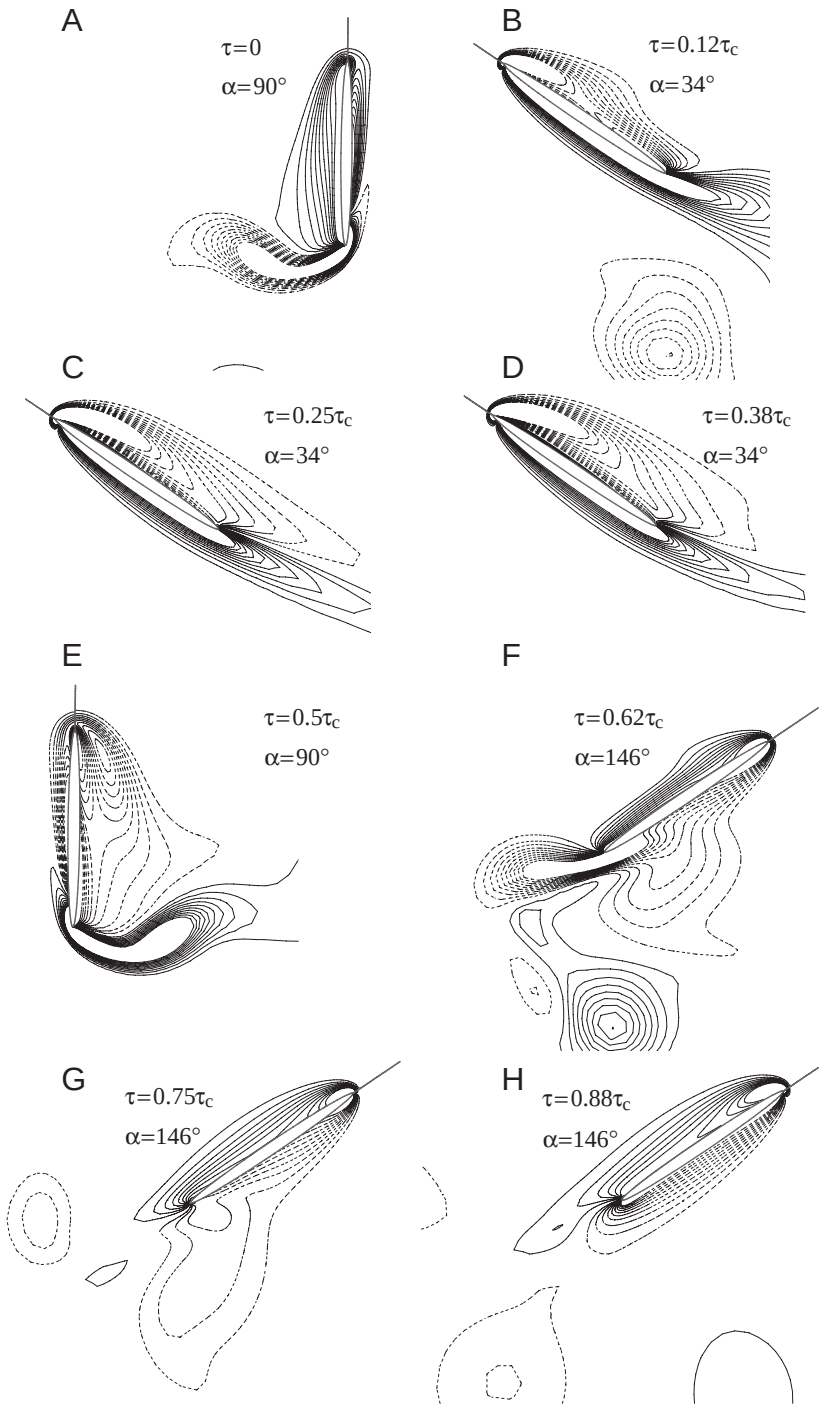

Fig. 5. (A–H) Vorticity plots at half-wing length at various times during one cycle (advance ratio J=0.27). τ is 60°, non-dimensional time; τ_c is 60°, non-dimensional period of one cycle; α, angle of attack of wing. Solid and broken lines indicate positive and negative vorticity, respectively. The magnitude of the non-dimensional vorticity at the outer contour is 1 and the contour interval is 1. (A–D), downstroke; (E–H), upstroke.

For the case of high flight speed (J=0.53; β=60°; α_m=56°), during the translatory phase of the downstroke (τ=0.09~0.41τ_c), even larger C_l and C_d are maintained. As seen in Fig. 6B–D (and Fig. 9A–C), the LEV does not shed, and again, maintaining the large C_l and C_d is due to the delayed stall mechanism. Because α_m is large in this case (56°), C_d is larger than C_l. During the translatory phase of the upstroke, both C_l and C_d are small, for the same reason as given above for the case of J=0.27. (In Fig. 9D–F, it is seen that during this period, the streamlines in front of the wing are almost aligned with the wing chord, i.e. the effective angle of attack is very small.)

It should be noted that the effective angle of attack varies during a downstroke or upstroke. For example, in Fig. 7 (J=0), during the downstroke (Fig. 7A–C), the effective angle of attack is small at the early part of the stroke (Fig. 7A), and becomes larger in the later part of the stroke (Fig. 7B,C); the same is true during the upstroke (Fig. 7D–F). (Similar variation of effective angle of attack during a down- or upstroke can be seen in Figs 8, 9). This is because, as explained in Birch and Dickinson (2001) and Sun and Tang (2002a), during the stroke reversal the wing rotation induced a downwash, which decreased the effective angle of attack of the wing in the early part of the following stroke.

The above discussion helps to explain the negative C_l at the early part of the upstroke in the cases of higher advance ratios (Fig. 3D, J=0.27–0.53). At higher advance ratios, β is relatively large, and so is the 'downwash' velocity due to V_∞. This 'downwash' velocity together with the induced downwash velocity by wing rotation makes the effective angle of attack to be around zero (see Figs 8D, 9D,E), resulting in the negative C_l.

Finally, we consider the wing drag C_d (see Fig. 3E). At low and medium flight speeds (J=0.13, 0.27), in the downstroke, the magnitude of C_d is larger than that of hovering (J=0), yet in the upstroke it is slightly smaller than that of hovering, indicating that the average of the magnitude of C_d over a flapping cycle is

a little smaller than that of hovering. But at high flight speed (J=0.53), in the downstroke, the magnitude of C_d is much larger than that of hovering, and in the upstroke, it is only a little smaller than that of hovering, indicating that the average of the magnitude of C_d over a cycle is much larger than that of hovering. Since the aerodynamic power is mainly determined by C_d (the inertial power for *Drosophila* is relatively small; Sun and Tang, 2002b), it is foreseen that the mechanical power at low and medium flight speeds is a little smaller that of hovering and increases rapidly at higher flight speeds.

Power required

As shown above, at a given flight speed, when α_m and β were properly chosen, the insect produced enough lift and thrust to support its weight and to overcome the body drag, respectively. We calculated the power required for production of the above lift and thrust, and investigated its properties and how it varied with the flight speed.

As expressed in equation 20 of Sun and Tang (2002b), the aerodynamic power consists of two parts, one due to the aerodynamic torque for translation and the other to the aerodynamic torque for rotation. The coefficients of these two torques, $C_{Q,a,t}$ and $C_{Q,a,r}$, are shown in Fig. 10A,B (for clarity, only the results for J=0, 0.27 and 0.53 are shown). $C_{Q,a,t}$ is much larger than $C_{Q,a,r}$. The $C_{Q,a,t}$ curve is similar in shape to the C_d curve shown in Fig. 3E, for obvious reasons.

The inertial power also consists of two parts (see equation 35 of Sun and Tang, 2002b). The coefficients of the inertial torques for translation ($C_{Q,i,t}$) and for rotation ($C_{Q,i,r}$) are shown in Fig. 10C,D. $C_{Q,i,t}$ does not vary with flight speed since the translational motion of the wing is the same for all flight speeds. $C_{Q,i,r}$ at J=0.53 is smaller than that at J=0 and 0.13, because at J=0.53, α_m is larger and the angle rotated at stroke reversal is smaller, thus $\dot{\alpha}^+$ is smaller.

With the above results for the aerodynamic and inertial torque coefficients, the power coefficients can be computed using equations 41–43 of Sun and Tang (2002b). The coefficients of power for translation ($C_{P,t}$) and for rotation ($C_{P,r}$) are plotted against the non-dimensional time in Fig. 11. Throughout a flapping cycle, the magnitude of $C_{P,t}$ is much larger than that of $C_{P,r}$. $C_{P,t}$ varies with flight speed in the same way as the wing drag coefficient C_d does. That is, at low to medium flight speeds (J=0.13–0.27), the average of $C_{P,t}$

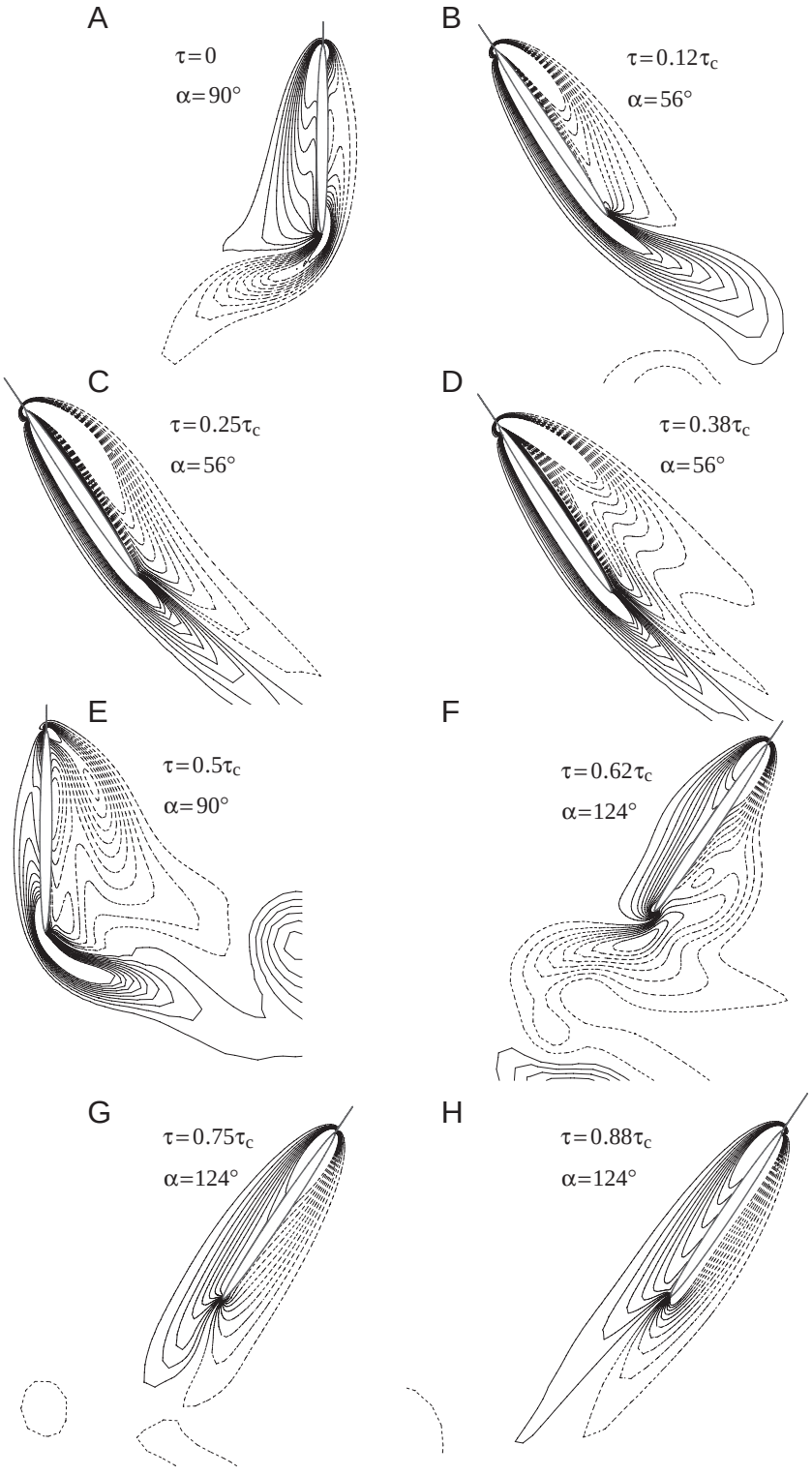

Fig. 6. (A–H) Vorticity plots at half-wing length at various times during one cycle (advance ratio J=0.53). τ is 60°, non-dimensional time; τ_c is 60°, non-dimensional period of one cycle; α, angle of attack of wing. Solid and broken lines indicate positive and negative vorticity, respectively. The magnitude of the non-dimensional vorticity at the outer contour is 1 and the contour interval is 1. (A–D), downstroke; (E–H), upstroke.

over a flapping cycle is a little smaller than that of hovering, but at high flight speed (J=0.53), the average of $C_{P,t}$ is much larger than that of hovering. This indicates that the power requirement at low to medium speeds is a little smaller than that of hovering, and becomes much larger at higher speeds.

From Fig. 11 it is also seen that at hovering (J=0), $C_{P,t}$ is the

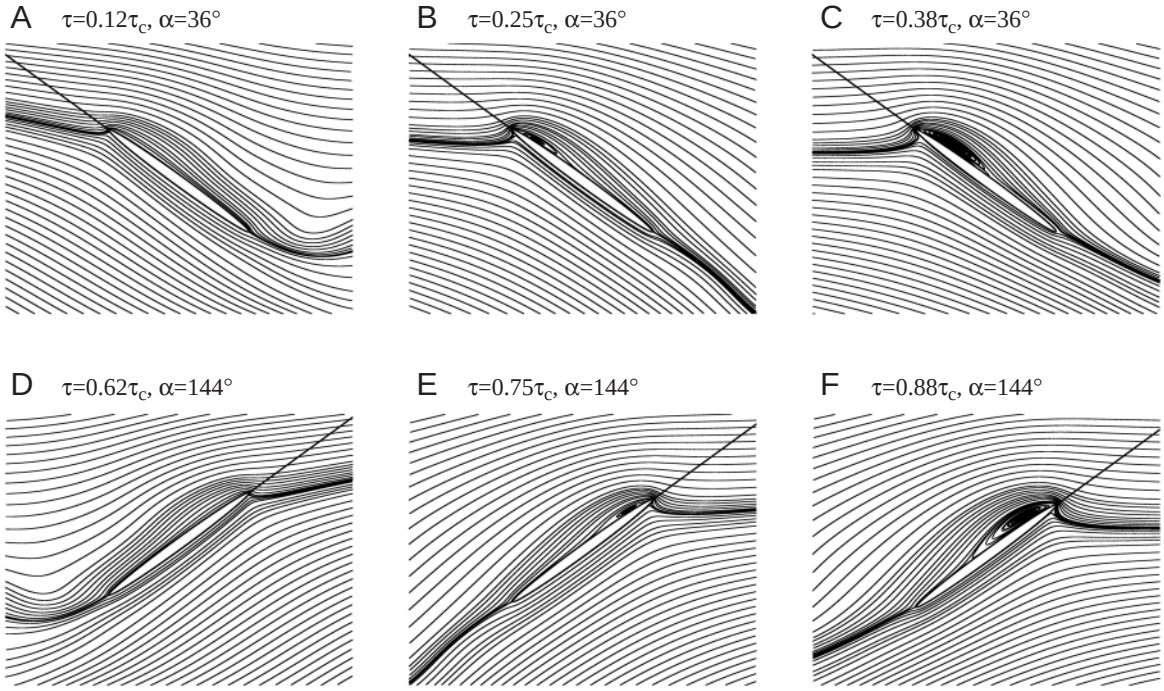

Fig. 7. Sectional streamline plots at half-wing length at various times during one cycle (advance ratio J=0). τ, non-dimensional time; τ_c, non-dimensional period of one cycle; α, angle of attack of wing (the spatial interval of the incoming streamlines can be seen from the left or right of a plot). (A–C), downstroke; (D–F), upstroke.

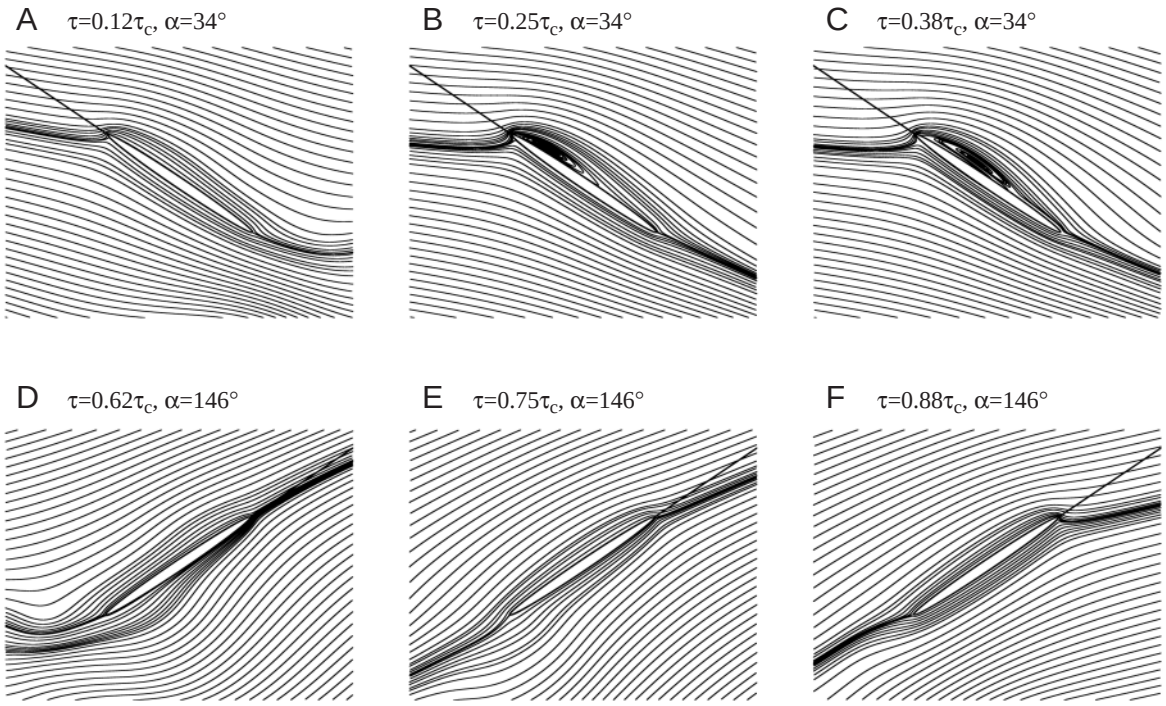

Fig. 8. Sectional streamline plots at half-wing length at various times during one cycle (advance ratio J=0.27). τ, non-dimensional time; τ_c, non-dimensional period of one cycle; α, angle of attack of wing (the spatial interval of the incoming streamlines can be seen from the left or right of a plot). (A–C), downstroke; (D–F), upstroke.

same during the down- and upstrokes, but at forward flight, especially at medium and high speeds (J=0.27–0.53), $C_{P,t}$ during the downstroke is much larger than $C_{P,t}$ during the upstroke. At J=0.13, 0.27 and 0.53, average values of $C_{P,t}$ over the downstroke are approximately 1.6, 2.6 and 3.5 times as much as that over the upstroke, respectively. This indicates that in forward flight, the flight muscle of the insect must do significantly more work during the downstroke than during the upstroke.

Integrating $C_{P,t}$ over the part of a wingbeat cycle where it is positive gives the coefficient of positive work for translation, which is represented by $C^{+}_{W,t}$. Integrating $C_{P,t}$ over the part of the cycle where it is negative gives the coefficient of 'negative' work for 'braking' the wing in this part of the cycle, which is represented by $C^{-}_{W,t}$. Similar integration of $C_{P,r}$ gives the coefficients of positive and negative work for rotation; and they are denoted by $C^{+}_{W,r}$ and $C^{-}_{W,r}$, respectively. The results of the integration are shown in Table 1.

The mass specific power, repressed by P*, is defined as the mean mechanical power over a flapping cycle divided by the mass of the insect m, and it can be written as follows:

$$P^* = 0.5\rho U^3 S_t \times (C_w/\tau_c) / m = 9.81U \times (C_w/\tau_c) / \overline{C_{L,w}}\,, \quad (10)$$

where C_w is the coefficient of work per cycle.

When calculating C_w, one needs to consider how the negative work fits into the power budget (Ellington, 1984c). There are three possibilities (Ellington, 1984c; Weis-Fogh, 1972, 1973). One is that the negative power is simply dissipated as heat and sound by some form of an end stop, then it can be ignored in the power budget. The second is that in the period of negative work, the excess energy can be stored by an elastic element, and this energy can then be released when the wing does positive work. The third is that the flight muscles do negative work (i.e. they are stretched while developing tension, instead of contracting as in 'positive' work) but the negative work uses much less metabolic energy than an equivalent amount of positive work. In the previous work on hovering flight (Sun and Tang, 2002b), out of these three possibilities, C_w was calculated based on the assumption that the muscles act as an end stop, i.e.:

$$C_w = C^{+}_{W,t} + C^{+}_{W,r}\,. \quad (11)$$

Sun and Tang (2002b) pointed out that for the insect considered, the negative work is much smaller than the positive work and C_w calculated by considering the other possibilities would not be very different from that by Equation 11. This is also true here, as seen from the values of $C_{W,t}{}^{-} + C^{-}_{W,r}$ in Table 1. Therefore, in the present study, Equation 11 is employed for calculation of C_w.

The calculated results of C_w are also given in Table 1. With C_w known, the specific power P* was computed using Equation 10, and is plotted against flight speed in Fig. 12 (see the circles in the figure). At J=0.13 and 0.27, P* is only approximately 10% smaller than that of hovering; at J=0.40, P* is about the same as that of hovering; but at J=0.53, P* is approximately 41% larger than that of hovering. As foreseen above (on the basis of the variation of C_d with flight speed),

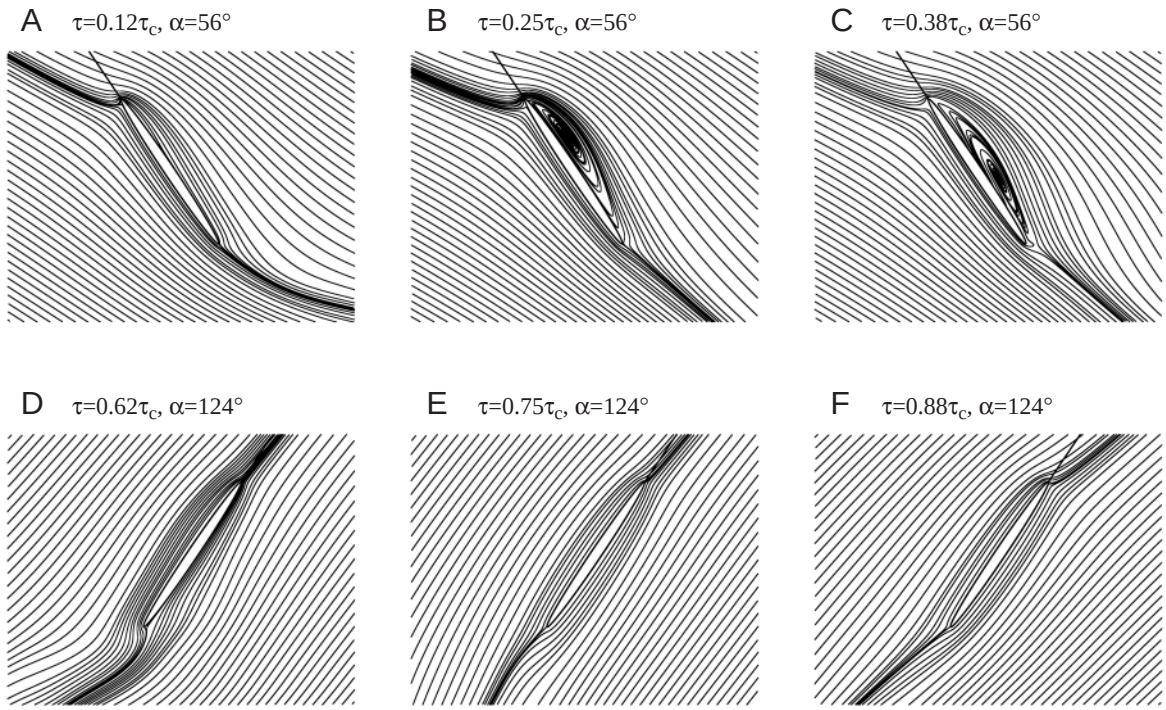

Fig. 9. Sectional streamline plots at half-wing length at various times during one cycle (advance ratio J=0.53). τ, non-dimensional time; τ_c, non-dimensional period of one cycle; α, angle of attack of wing (the spatial interval of the incoming streamlines can be seen from the left or right of a plot). (A–C), downstroke; (D–F), upstroke.

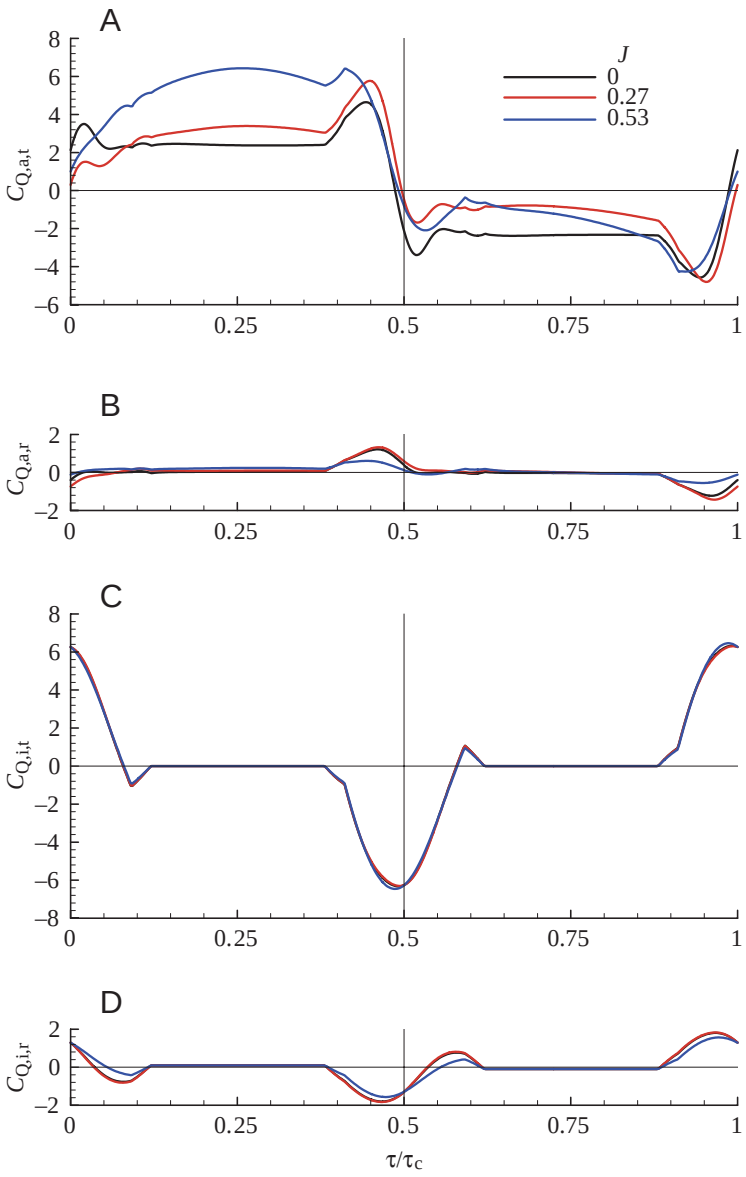

Fig. 10. Aerodynamic torque coefficients for translation $C_{Q,a,t}$ (A) and for rotation $C_{Q,a,r}$ (B) and inertial torque coefficients for translation $C_{Q,i,t}$ (C) and for rotation $C_{Q,i,r}$ (D) *versus* time in one cycle for various advance ratios J. τ, non-dimensional time; τ_c, non-dimensional period of one cycle.

the power requirement at low to intermediate speeds is a little smaller than that of hovering, and it increases rapidly at higher flight speeds.

The case of stroke amplitude and stroke plane angle varying with flight speed

In the above calculations, the midstroke angle of attack of the wing α_m and the stroke plane angle β were allowed to vary with flight speed but the stroke amplitude Φ and stroke frequency n were assumed constant. In this section, we considered the case in which the stroke amplitude Φ and stroke plane angle β were allowed to vary with flight speed but α_m and n were assumed constant. Vogel (1967) observed that the geometrical angle of attack of *Drosophila virilis* in tethered flight did not vary with flight speed, and that it was between 40° and 50° (see fig. 4 of Vogel, 1967); here we took α_m as 46.5°. (Other parameters were the same as in the above case.)

For a given flight speed, Φ and β were chosen such that the lift and thrust balanced the insect weight and the body drag, respectively. The calculation procedure was similar to that in the case of α_m and β varying with flight speed (see above).

The calculated $\overline{C_L}$, $\overline{C_T}$, Φ and β as functions of flight speed or advance ratio are shown in Table 2. It is seen, as when α_m and β vary with flight speed, β increases almost linearly with flight speed, and in both cases β is almost the same (compare the β values in Table 2 and Table 1). Φ is close to that of hovering flight at low flight speeds (J=0.13, 0.27) but increases to large values at higher speeds; Φ varies with flight speed in the same way as α_m did in the case of α_m and β varying with flight speed. (As seen Table 2, we again only have results up to J=0.53. At a higher flight speed, J=0.66, no matter how Φ and β were adjusted, enough lift could not be obtained.)

The lift (vertical force) and thrust coefficients (C_L and C_T) *versus* non-dimensional time for various advance ratios are shown in Fig. 13B,C. They are similar to their counterparts in the case of α_m and β varying with flight

Table 2. *Mean lift ($\overline{C}_L$) and thrust ($\overline{C}_T$) coefficients, stroke amplitude Φ, stroke plane angle β, body angle χ and coefficient of work per cycle C_w as functions of advance ratio* J

J	$\overline{C}_L$	$\overline{C}_T$	Φ (deg.)	β (deg.)	χ (deg.)	C_w	$C^+_{W,t}$	$C^-_{W,t}$	$C^+_{W,r}$	$C^-_{W,r}$
0	1.15	0.03	135	0	68	14.09	13.99	–0.99	0.10	–1.98
0.13	1.15	0.04	129	18.5	49.5	12.67	12.56	–0.74	0.11	–1.66
0.27	1.15	0.08	131	34.5	33.5	12.01	11.89	–0.68	0.12	–1.55
0.40	1.15	0.14	145	47	21	13.63	13.49	–0.75	0.14	–1.69
0.53	1.16	0.20	165	53	15	17.57	17.41	–0.97	0.16	–2.05

Φ, β vary with flight speed; α_m=46.5°; n=240 s^{-1} and non-dimensional period τ_c=8.42.

$C^+_{W,t}$ and $C^-_{W,t}$, coefficients of positive and negative work for translation, respectively; $C^+_{W,r}$ and $C^-_{W,r}$, coefficients of positive and negative work for rotation, respectively.

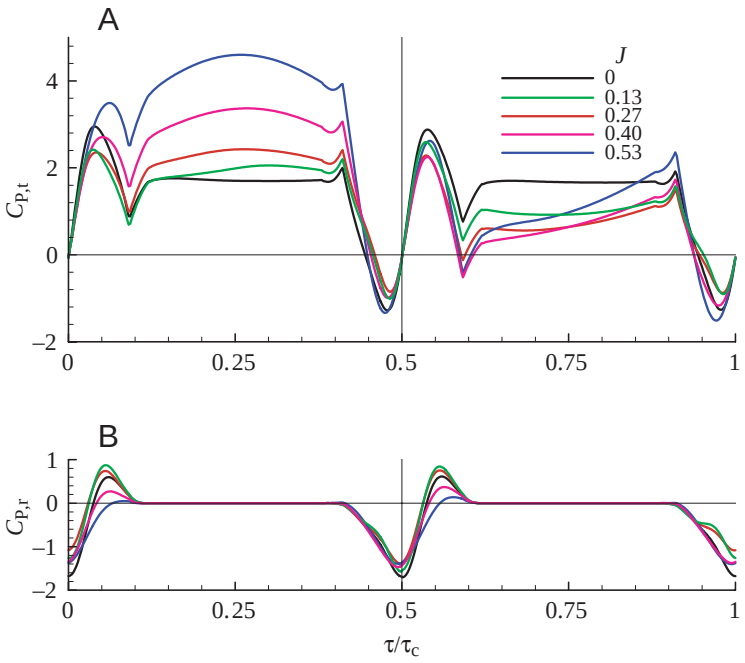

Fig. 11 Coefficients of power for translation $C_{P,t}$ (A) and for rotation $C_{P,r}$ (B) *versus* time in one cycle for various advance ratios *J*. τ, non-dimensional time; τ_c, non-dimensional period of one cycle (midstroke angle of attack α_m and stroke plane angle β vary with flight speed; stroke amplitude Φ=150°).

speed (see Fig. 3B,C). At low flight speed (*J*=0.13), both the down- and upstrokes contribute to the mean lift but approximately 80% of the mean lift is from the downstroke; the mean thrust is contributed by the upstroke (the downstroke has negative contribution). At medium flight speed (*J*=0.27), the mean lift is contributed by the downstroke, and the mean thrust is contributed by the upstroke (the downstroke has negative contribution). At high flight speed (*J*=0.53), the mean lift is contributed by the downstroke (the upstroke has a small negative contribution), and the mean thrust is contributed almost equally by the down- and upstrokes (in the case of α_m and β varying with flight speed, at high flight speed, the upstroke has relatively large contribution to the mean thrust).

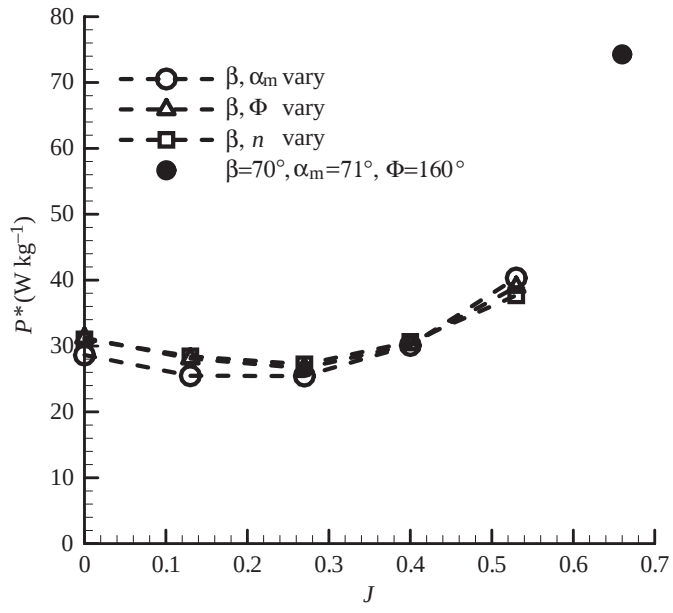

Fig. 12. Body-mass-specific power P^* *versus* advance ratios *J*. α_m, midstroke angle of attack; β, stroke angle; Φ, stroke amplitude; *n*, stroke frequency.

The wing lift and drag coefficients (C_l, C_w and $C_{d'}$) *versus* non-dimensional time for various advance ratios are shown in Fig. 13D–F, and are also similar to their counterparts in the case of α_m and β varying with flight speed (see Fig. 3D–F). Using the flow field information (vorticity contours and streamline patterns around the wing), it was shown that the mechanisms operating in the generation of C_l and C_d in the present case were the same as that in the case of α_m and β varying with flight speed.

The coefficients of power for translation and for rotation *versus* non-dimensional time are shown Fig. 14; again they are very similar to their counterparts in the case of α_m and β varying with flight speed (see Fig. 11). At low speed (*J*=0.13), medium speed (*J*=0.27) and high speed (*J*=0.53), the average values of $C_{P,t}$ over the downstroke are approximately 1.6, 2.8 and 4.2 times as large as that over the upstroke, respectively.

The coefficients of work per cycle (C_w), calculated in the same way as in last section, are shown in Table 2. With C_w, the specific power P^* was computed and the results shown Fig. 12 (triangles). It is seen that P^* in the present case is approximately the same as that in the case of α_m and β varying with flight speed.

The case of stroke frequency and stroke plane angle varying with flight speed

In this section, we consider the case in which the stroke frequency *n* and stroke plane angle β were allowed to vary with flight speed (α_m and Φ were assumed constant; α_m=46.5°, Φ=150°; other parameters were the same as in the above two cases).

For a given flight speed, *n* and β were chosen such that lift and thrust balance the insect weight and body drag, respectively. The calculation procedure was similar to that in the case of Φ and β varying with flight speed).

The calculated C_L, C_T, *n*, β and C_w as functions of advance ratio are shown in Table 3. (Similar to the above two cases, we have results up to *J*=0.53. At *J*=0.66, no matter how *n* and β were adjusted, enough lift could not be obtained.) Comparing the results in Table 3 (*n* varying with flight speed) and in Table 2 (Φ varying with flight speed) shows that *n* varies with flight speed in the same way as Φ does in their respective cases. Note that at each of the advance ratios (or flight speeds) considered, *n*Φ is approximately the same for the two cases. This shows that (in the range of Φ and *n* considered in the

Table 3. *Mean lift ($\bar{C}_L$) and thrust ($\bar{C}_T$) coefficients, stroke frequency* n *(and non-dimensional period τ_c), stroke plane angle β, body angle χ and coefficient of work per cycle* C_w *as functions of advance ratio* J

J	$\bar{C}_L$	$\bar{C}_T$	n (s^{-1})	τ_c	β (deg.)	χ (deg.)	C_w	$C^+_{W,t}$	$C^-_{W,t}$	$C^+_{W,r}$	$C^-_{W,r}$
0	1.14	0.02	216	9.32	0	68	15.54	15.49	–0.52	0.05	–1.17
0.13	1.14	0.06	208	9.72	18	50	14.87	14.81	–0.39	0.06	–0.99
0.27	1.15	0.08	210	9.58	31	37	14.03	13.98	–0.28	0.05	–0.79
0.40	1.16	0.15	232	8.68	46	22	14.29	14.21	–0.29	0.08	–0.85
0.53	1.14	0.19	264	7.62	58	10	15.44	15.26	–0.36	0.18	–1.00

n, β vary with flight speed; α_m=46.5°; Φ=150°.

$C^+_{W,t}$ and $C^-_{W,t}$, coefficients of positive and negative work for translation, respectively; $C^+_{W,r}$ and $C^-_{W,r}$, coefficients of positive and negative work for rotation, respectively.

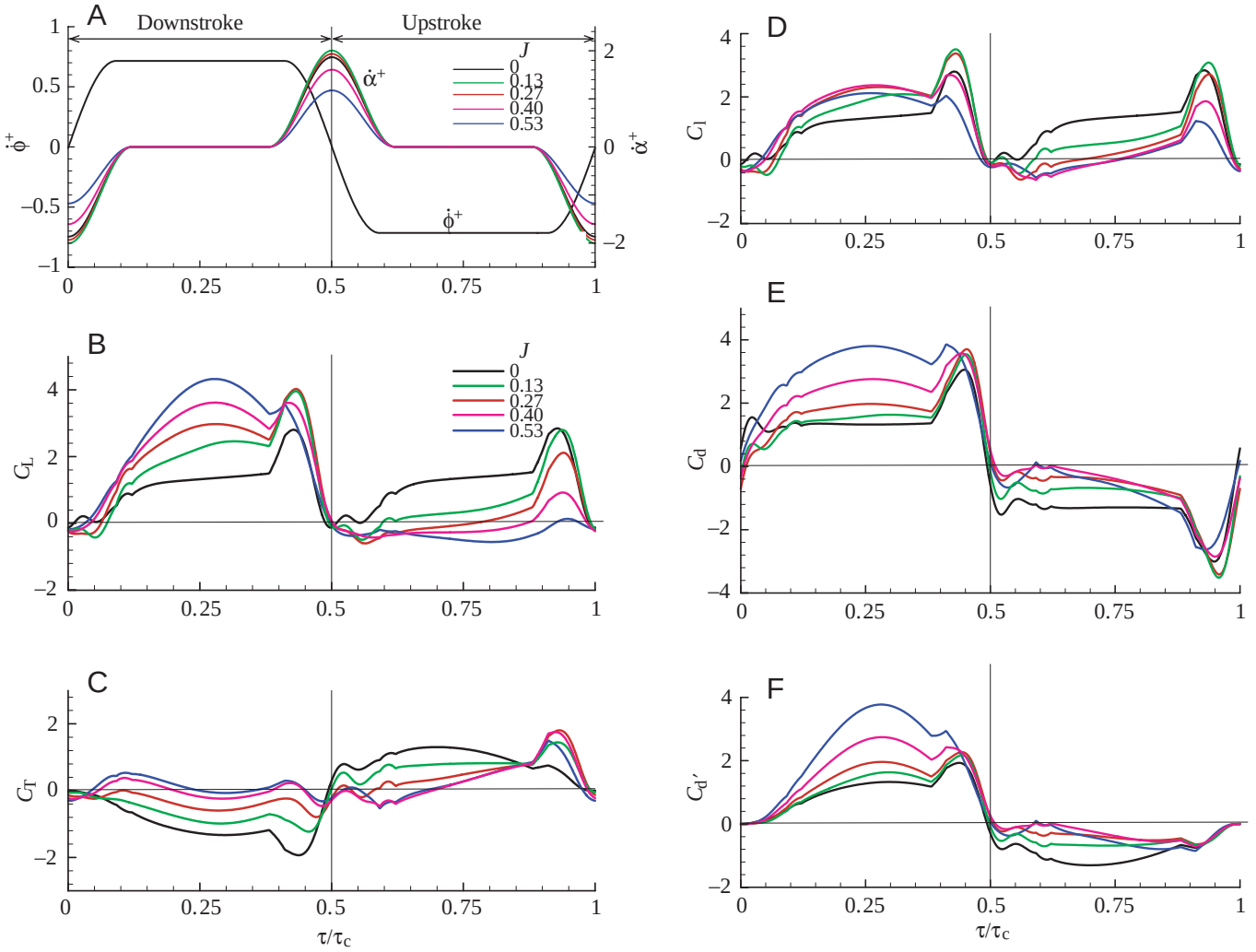

Fig. 13. Non-dimensional angular velocity of pitching rotation $\dot{\alpha}^+$ and azimuthal rotation $\dot{\phi}^+$ (A), lift coefficient C_L (B), thrust coefficient C_T (C), wing lift coefficient C_l (D), wing drag coefficient C_d (E) and x' component of wing drag coefficient $C_{d'}$ (F) *versus* time during one cycle for five advance ratios J. τ_c, non-dimensional period of one flapping cycle; τ, non-dimensional time (stroke amplitude Φ and stroke plane angle β vary with flight speed; midstroke angle of attack α_m=46.5°; stroke frequency n=240 s^{-1}).

present study), the insect can change its Φ or n by approximately the same percentage to produce a similar change of aerodynamic force. The reason for this is obvious: the aerodynamic force is approximately proportional to the square of the translational velocity of the wing, which is proportional to $n\Phi$.

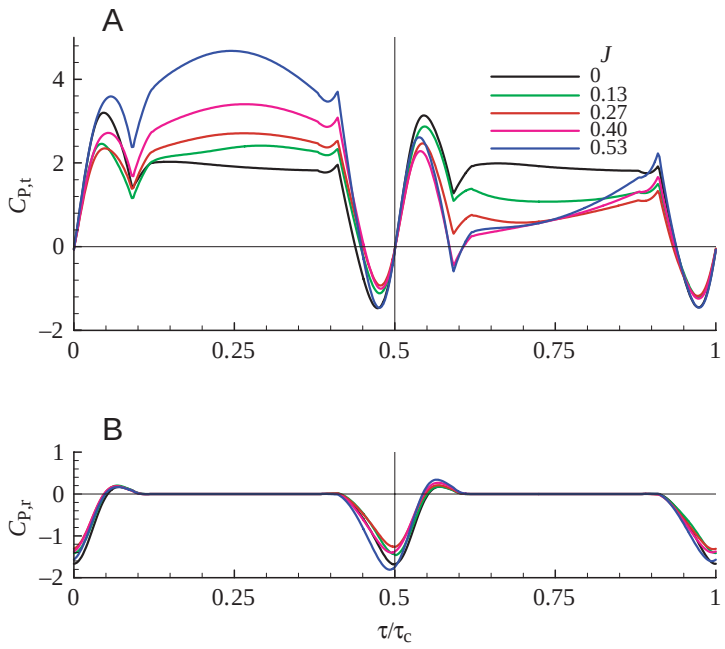

Fig. 14. Coefficients of power for translation $C_{P,t}$ (A) and for rotation $C_{P,t}$ (B) *versus* time in one cycle for various advance ratios J. τ, non-dimensional time; τ_c, non-dimensional period of one cycle (stroke amplitude Φ and stroke plane angle β vary with flight speed; midstroke angle of attack α_m=46.5°; stroke frequency n=240 s^{-1}).

The specific power P^* is given in Fig. 12 (see the squares in the figure). P^* is almost the same as that in the other two cases.

An additional case

In the above analyses, we considered three cases where α_m, β, Φ and n varied with flight speed. In the first case, α_m and β varied with flight speed and Φ and n were constant (Φ=150°, n=240 s^{-1}); in the second case, Φ and β varied with flight speed and α_m and n were constant (α_m=46.5°, n=240 s^{-1}); in the third case, n and β varied with flight speed and α_m and Φ were constant (α_m=46.5°,Φ=150°). In all the three cases, when the advance ratio was increased to J=0.66 (V_∞=2.5 m s^{-1}), enough lift to balance the weight could not be obtained. For reference, we conducted an additional calculation at J=0.66, in which Φ, α_m and β could be adjusted (n fixed as 240 s^{-1}).

It was shown that when Φ=160°, α_m=71° and β=70°, the lift and thrust balanced the weight and the body drag, respectively. The thrust coefficient C_T was 0.27; the body angle χ was –2°. The specific power P^* was included in Fig. 12 (see the dot in the figure); it is about three times as large as that of hovering, and it is believed that the insect does not fly at such a speed for flights of long duration.

Comparisons between the present results and previous data

LEV and delayed stall mechanism in forward flight

Flow visualization on tethered hawkmoth (Ellington et al., 1996; Willmott et al., 1997) showed that even at high speeds, when the wing traveled a large distance during downstroke (more than 6 chord lengths), the LEV did not shed in the translatory phase of the stroke. In the present work, we show that this also true for the model fruit fly wing. At high speeds (J=0.53, 0.66), a wing section at half-wing length travels approximately 6.5 chord lengths during downstroke and the LEV did not shed. Here, chord lengths travelled during downstroke, Λ_d, is approximately estimated by the following formula:

$$\Lambda_d = 0.5\Phi R/c + V_\infty \cos\beta/2nc = 0.5\Phi R/c + J\cos\beta\Phi R/c \, . \quad (12)$$

For example, using data of the model fruit wing (Φ=150°, R/c=3), when J=0.53 and β=53°, Λ_d is 6.6.

The present results complement the flow visualization on the hawkmoth in two ways. One is that the wings of the hawkmoth and that of the fruit fly operated at Reynolds numbers of about 4000 and 100, respectively, and the Reynolds number of most insects are between these two values; this indicates that the delayed stall mechanism applies to most insects in both hovering and forward flight. The other is that the flow visualization pictures for the tethered hawkmoth were not so clearcut because of the difficulty in obtaining good flow visualization near the wings of the insect, but the present CFD-visualized LEV was clear. [Liu et al. (1998) presented CFD-visualized LEV on a model wing of the hawkmoth, but only for the case of hovering flight.]

The aerodynamic and energetic roles of the down- and upstrokes

Dudley and Ellington (1990a,b) systematically studied the kinematics, lift and power requirements of forward flight in bumblebees. On the basis of wing kinematics and quasi-steady aerodynamic theory, they demonstrated that the downstoke progressively became more important in production of the lift (vertical force) as flight speed increased. They considered that quantitative treatment of the relative contributions to the thrust generation of the downstroke and upstroke was not possible at the time, because the condition of horizontal force balance could not be satisfied in the analysis. In a subsequent paper by Ellington (1995), on the basis of a further analysis of the data from Dudley and Ellington (1990a), it was demonstrated that, as the advance ratios increased, the downstroke would increasingly dominate weight support, and that the upstroke contributed thrust at all speeds but its contribution decreased with increasing forward speed, a trend that was offset by an increasing thrust component from the downstroke force.

The present results on the aerodynamic roles of the down- and upstrokes of the *Drosophila virilis* in forward flight are in agreement with those of bumblebees by Dudley and Ellington (1990a,b) and Ellington (1995), although the results for bumblebees were based on steady-state aerodynamic analysis.

In previous studies on power requirements of forward flight of insects, to the author's knowledge, the relative contributions

to the mechanical power of the downstroke and the upstroke were not mentioned (only the mean power over a flapping cycle was presented). The present study (see Figs 11, 14) showed that although in hovering with a horizontal stroke plane the work done in the downstroke was the same as that in the upstroke, in forward flight, even at low flight speed, the work done in the downstroke was considerably more than that done in the upstroke. In the case of β and Φ varying with flight speed, at advance ratios J=0.13, 0.27 and 0.53, the work done in the downstroke was approximately 1.6, 2.8 and 4.2 times as much as that in the upstroke.

Graph of mechanical power against flight speed approximately J-shaped

The measured oxygen consumption of bumblebees and a hummingbird in forward flight showed little dependence of metabolic power on speed from hovering to intermediate speeds, and for the hummingbird, a sharp increase at higher speeds (measurement for bumblebees at higher speeds are not available; for a review, see Ellington, 1991). If the muscle efficiency of the animals is assumed constant over various speeds, the mechanical power would vary with speed according to a J-shaped curve (Ellington et al., 1990; Ellington, 1991).

From results of the present study, this is approximately true for fruit fly *Drosophila virilis*. As illustrated in Fig. 12, at hovering, the body mass-specific power P^* is approximately 29 W kg^{-1}; at J=0.13 and 0.27, P^* is only approximately 10% less than that of hovering; at J=0.4, P^* is almost the same as that of hovering; but when J is furthered increased, P^* has a sharp increase (at J=0.53, P^* is approximately 40% larger than that of hovering, and at J=0.66, P^* is approximately 150% larger than that of hovering). That is, the graph of the specific power against flight speed is approximately J-shaped.

Speed for fast flight

From Fig. 13, it is seen that at J=0.4, the power is a little larger than that at lower speeds and is almost the same as that of hovering, and afterwards the power increases sharply. This indicates that the insect would usually fly at advance ratios between 0 and 0.4, and that for fast flight, it would fly at an advance ratio around 0.4. (Flying at higher advance ratios would be very energy-demanding.) No data are available for *Drosophila virilis* in free forward flight; there exist some data for *Drosophila melanogaster*, however. Ennos (1989) observed *D. melanogaster* flying at J=0.33. Marden et al. (1997) showed that the upper limit of *D. melanogaster* flight speed was around 0.85 m s^{-1}. The corresponding advance ratio is around 0.32, estimated using the measured (Ennos, 1989) stroke angle (150°) and stroke frequency (254 s^{-1}) of free flying *D. melanogaster* (wing length R=2 mm). David (1978) recorded a maximum advance ratio of about 0.4 for *D. melanogaster* in experimental setting. The present computed results are consistent with these observations.

List of symbols

c	mean chord length
C_d	wing drag coefficient
$C_{d,'}$	x'-component of the wing drag coefficient
C_l	wing lift coefficient
$\underline{C_L}$	lift coefficient
$\overline{C_L}$	mean lift coefficient
$C_{L,W}$	mean lift coefficient for supporting the insect weight
$C_{P,r}$	coefficient of power for rotation
$C_{P,t}$	coefficient of power for translation
$C_{Q,a,r}$	coefficient of aerodynamic torque for rotation
$C_{Q,a,t}$	coefficient of aerodynamic torque for translation
$C_{Q,i,r}$	coefficient of inertial torque for rotation
$\underline{C_{Q,i,t}}$	coefficient of inertial torque for translation
$\overline{C_T}$	mean thrust coefficient
C_w	coefficient of work per cycle
$C^+_{W,r}$	coefficient of positive work for rotation
$C^-_{W,r}$	coefficient of negative work for rotation
$C^+_{W,t}$	coefficient of positive work for translation
$C^-_{W,t}$	coefficient of negative work for translation
d	wing drag
d'	x'-component of the wing drag
J	advance ratio
l	wing lift
L	lift
m	mass of the insect
n	flapping frequency
O, o', o	origins of the two inertial frames of reference and the non-inertial frame of reference
p	non-dimensional fluid pressure
P^*	body mass-specific power
r_2	radius of the second moment of wing area
R	wing length
Re	Reynolds number
S	area of one wing
S_t	area of a wing pair
t	time
T	thrust
u_t	translational velocity of the wing
u_t^+	non-dimensional translational velocity of the wing
U	reference velocity
U_m	midstroke translational velocity of wing (or maximum of μ)
U_m^+	maximum of u_t^+
V_∞	free-stream velocity
X, Y, Z	coordinates in inertial frame of reference (Z in vertical direction)
x', y', z'	coordinates in inertial frame of reference (z' perpendicular to stroke plane)
x, y, z	coordinates in non-inertial frame of reference
α	geometric angle of attack
α_m	midstroke geometric angle of attack
$\dot{\alpha}$	angular velocity of pitching rotation

$\dot{\alpha}^+$	non-dimensional angular velocity of pitching rotation
$\dot{\alpha}_0{}^+$	a constant
β	stroke plane angle
$\Delta\tau_t$	duration of deceleration/acceleration around stroke reversal (non- dimensional)
$\Delta\tau_r$	duration of wing rotation or flip duration (non-dimensional)
Λ_d	chord lengths traveled by a wing section at half-wing length during downstroke
ν	kinematic viscosity
ρ	density of fluid
τ	non-dimensional time
τ_0	time when a stroke starts (non-dimensional)
τ_1	time when translational deceleration starts (non-dimensional)
τ_r	time when pitching rotation starts (non-dimensional)
τ_c	period of one flapping cycle (non-dimensional)
Φ	stroke amplitude
ϕ	azimuthal or positional angle
$\dot{\phi}$	angular velocity of azimuthal rotation
$\dot{\phi}^+$	non-dimensional angular velocity of azimuthal rotation
χ	body angle

We thank the two referees whose helpful comments and valuable suggestions greatly improved the quality of the paper. This research was supported by the National Natural Science Foundation of China.

References

Birch, J. M. and Dickinson, M. H. (2001). Spanwise flow and the attachment of the leading-edge vortex on insect wings. *Nature* **412**, 729-733.

David, C. T. (1978). The relationship between body angle and flight speed in free-flying *Drosophila*. *Phys. Ent*. **3**, 191-195.

Dickinson, M. H. (1994). The effects of wing rotation on unsteady aerodynamic performance at low Reynolds numbers. *J. Exp. Biol.* **192**, 179-206.

Dickinson, M. H. and Götz, K. G. (1993). Unsteady aerodynamic performance of model wings at low Reynolds numbers. *J. Exp. Biol.* **174**, 45-64.

Dickinson, M. H., Lehman, F. O. and Sane, S. P. (1999). Wing rotation and the aerodynamic basis of insect flight. *Science* **284**, 1954-1960.

Dudley, R. and Ellington, C. P. (1990a). Mechanics of forward flight in bumblebees. I. Kinematics and morphology. *J. Exp. Biol.* **148**, 19-52.

Dudley, R. and Ellington, C. P. (1990b). Mechanics of forward flight in bumblebees. II. Quasi-steady lift and power requirements. *J. Exp. Biol.* **148**, 53-88.

Ellington, C. P. (1984a). The aerodynamics of hovering insect flight. III. Kinematics. *Phil. Trans. R. Soc. Lond. B* **305**, 41-78.

Ellington, C. P. (1984b). The aerodynamics of hovering insect flight. IV. Aerodynamic mechanisms. *Phil. Trans. R. Soc. Lond. B* **305**, 79-113.

Ellington, C. P. (1984c). The aerodynamics of hovering insect flight. VI. Lift and power requirements. *Phil. Trans. R. Soc. Lond. B* **305**, 145-181.

Ellington, C. P. (1991). Limitations on animal flight performance. *J. Exp. Biol.* **160**, 71-91.

Ellington, C. P. (1995). Unsteady aerodynamics of insect flight. In *Biological Fluid Dynamics. Symp. Soc. Exp. Biol*. **49** (ed. C. P. Ellington and T. J. Pedley), pp. 109-129. Cambridge: Company of Biologists.

Ellington, C. P., Machin, K. E. and Casey, T. M. (1990). Oxygen consumption of bumblebees in forward flight. *Nature* **347**, 472-473.

Ellington, C. P., van den Berg, C. and Willmott, A. P. (1996). Leading edge vortices in insect flight. *Nature* **384**, 626-630.

Ennos, A. R. (1989). The kinematics and aerodynamics of the free flight of some Diptera. *J. Exp. Biol.* **142**, 49-85.

Fung, Y. C. (1969). *An Introduction to the Theory of Aeroelasticity*. New York: Dover.

Lan, S. L. and Sun, M. (2001a). Aerodynamic of properties of a wing performing unsteady rotational motions at low Reynolds number. *Acta Mech.* **149**, 135-147.

Lan, S. L. and Sun, M. (2001b). Aerodynamic interaction between two airfiols in unsteady motions. *Acta Mech.* **150**, 39-51.

Lehmann, F.-O. and Dickinson, H. D. (1997). The changes in power requirements and muscle efficiency during elevated force production in the fruit fly *Drosophila melanogaster*. *J. Exp. Biol.* **200**, 1133-1143.

Liu, H., Ellington, C. P., Kawachi, K., Van Den Berg, C. and Willmott, A. P. (1998). A computational fluid dynamic study of hawkmoth hovering. *J. Exp. Biol.* **201**, 461-477.

Marden, J. H., Wolf, M. R. and Weber, K. E. (1997). Aerial performance of *Drosophila melanogaster* from populations selected for upwind flight ability. *J. Exp. Biol.* **200**, 2747-2755.

Rogers, S. E. and Kwak, D. (1990). Upwind differencing scheme for the time-accurate incompressible Navier–Stokes equations. *AIAA J.* **28**, 253-262.

Rogers, S. E., Kwak, D. and Kiris, C. (1991). Numerical solution of the incompressible Navier–Stokes equations for steady-state and dependent problems. *AIAA J.* **29**, 603-610.

Sane, S. P. and Dickinson, M. H. (2001). The control of flight force by a flapping wing: lift and drag production. *J. Exp. Biol.* **204**, 2607-2626.

Sane, S. P. and Dickinson, M. H. (2002). The aerodynamic effects of wing rotation and a revised quasi-steady model of flapping flight. *J. Exp. Biol.* **205**, 1087-1096.

Sun, M. and Tang, J. (2002a). Unsteady aerodynamic force generation by a model fruit fly wing in flapping motion. *J. Exp. Biol.* **205**, 55-70.

Sun, M. and Tang, J. (2002b). Lift and power requirements of hovering flight in *Drosophila*. *J. Exp. Biol.* **205**, 2413-2427.

Vogel, S. (1966). Flight in *Drosophila*. I. Flight performance of tethered flies. *J. Exp. Biol.* **44**, 567-578.

Vogel, S. (1967). Flight in *Drosophila*. II. Variations in stroke parameters and wing contour. *J. Exp. Biol.* **46**, 383-392.

Wang, Z. J. (2000). Two dimensional mechanism for insect hovering. *Phys. Rev. Lett.* **85**, 2216-2219.

Weis-Fogh, T. (1972). Energetics of hovering flight in hummingbirds and in *Drosophila*. *J. Exp. Biol.* **56**, 79-104.

Weis-Fogh, T. (1973). Quick estimates of flight fitness in hovering animals, including novel mechanism for lift production. *J. Exp. Biol.* **59**, 169-230.

Willmott, A. P. and Ellington, C. P. (1997a). The mechanics of flight in the hawkmoth *Manduca sexta*. I. Kinematics of hovering and forward flight. *J. Exp. Biol.* **200**, 2705-2722.

Willmott, A. P. and Ellington, C. P. (1997b). The mechanics of flight in the hawkmoth *Manduca sexta*. II. Aerodynamic consequences of kinematic and morphological variation. *J. Exp. Biol.* **200**, 2723-2745.

Willmott, A. P., Ellington, C. P. and Thomas A. R. (1997). Flow visualization and unsteady aerodynamics in the flight of the hawkmoth, *Manduca sexta*. *Trans. R. Soc. Lond. B* **352**, 303-316.

Wu, J. C. (1981). Theory for aerodynamic force and moment in viscous flows. *AIAA J.* **19**, 432-441.